

MEASUREMENT OF THE ADSORPTION KINETICS OF CO AND CO
CO-ADSORBED WITH O₂ ON Cr(110)

THESIS

Presented to the Graduate Council of
Texas State University-San Marcos
in Partial Fulfillment
of the Requirements

for the Degree

Master of SCIENCE

by

Jennifer L. Walters, B.S.

San Marcos, Texas
May 2010

MEASUREMENT OF THE ADSORPTION KINETICS OF CO AND CO
CO-ADSORBED WITH O₂ ON Cr(110)

Committee Members Approved:

Carl A. Ventrice, Jr., Chair

Heike Geisler

Ravindranath Droopad

Approved:

J. Michael Willoughby
Dean of the Graduate College

COPYRIGHT

by

Jennifer L. Walters

2010

ACKNOWLEDGEMENTS

I would like to thank my father and mother for always standing behind me and encouraging me to try my best in what ever endeavor I seek. To my brother James, you always put a smile on my face when I'm feeling the worst. To all my Aunts and Uncles, thank you for all the support you have given over the years. To my best friend Theresa, you helped keep me sane through all my academic struggles. You're like a sister to me. To all my friends and roommates, for keeping me going day to day and for the much needed breaks from physics. I'm here because you are all my foundation, my rock. Thank you all for your unending love and support. To my classmates Simona, Rob, Nick, Chris, and Gabe, I would not have been able to handle the workload without you. I'll never forget all the long crazy nights of unending homework. To Heike, you kept me motivated during this entire process. Thank you for all your help and support.

To my advisor Carl, I don't know anyone that works as hard as you. Your knowledge, work ethic, and enthusiasm are what I aspire to. I've learned more from you than any other professor at University. Thank you for your dedication and guidance.

This manuscript was submitted on December 16, 2009.

TABLE OF CONTENTS

	Page
ACKNOWLEDGEMENTS	iv
LIST OF FIGURES	vi
ABSTRACT	ix
 CHAPTER	
I. INTRODUCTION	1
A. Motivation	1
B. Previous Studies	1
II. INSTRUMENTATION AND THEORY	4
A. Ultra High Vacuum Chamber	4
B. Low Energy Electron Diffraction	8
C. Quadrupole Mass Spectrometer	14
D. Sample Holder	16
E. Temperature Programmed Desorption	19
F. Sample Preparation Technique	23
III. RESULTS	26
A. Adsorption of CO on mixed Cr ₂ O ₃ (0001) and Cr(110)	26
B. Adsorption of CO on Cr(110)	33
C. Co-adsorbed of CO with O ₂	44
IV. DISCUSSION	55
V. CONCLUSIONS	59
REFERENCES	61

LIST OF FIGURES

Figure	Page
1. Top View of Cr(110)	3
2. Side View of Cr(110)	3
3. Side View of the Experimental Chamber	7
4. Mean Free Path of the Electron	8
5. LEED Scattering Geometry	9
6. LEED Schematic	11
7. (110) Plane of a bcc Structure	12
8. Cr(110) Reciprocal Lattice	13
9. QMS Schematic	15
10. Quadrupole Mass Spectrometer and Interface Unit	16
11. Front View of the Experimental Chamber	17
12. Sample Holder	19
13. Ion Gun and High Voltage	24
14. Leak Valves	25
15. LEED images at 75 eV	27
16. Partial Pressure vs. Temperature curve of CO on different substrates	28
17. Partial Pressure vs. Partial Temperature curve for four consecutive dosing of CO on mixed Cr ₂ O ₃ (0001) and Cr(110)	30

18. Partial Pressure vs. Temperature curve of various masses measured for 1L dosing of CO on mixed Cr ₂ O ₃ (0001) and Cr(110)	31
19. Partial Pressure vs. Temperature curve of three consecutive dosing for 1L CO on mixed Cr ₂ O ₃ (0001) and Cr(110)	32
20. LEED images of clean Cr(110)	34
21. LEED images of 1L CO at 300 K on Cr(110)	35
22. Partial Pressure vs. Temperature curves of various masses for dosing 1L CO on Cr(110)	38
23. Pressure vs. Temperature curves of four consecutive dosing for 0.5L of CO on Cr(110)	39
24. Partial Pressure vs. Temperature curves of three consecutive dosing of 1L CO on Cr(110)	40
25. Partial Pressure vs. Temperature curves for three consecutive dosing of 5L CO on Cr(110)	41
26. Partial Pressure vs. Temperature curves for three consecutive dosing of 10L CO on Cr(110)	42
27. Partial Pressure vs. Temperature curves of five different dosing of CO on Cr(110)	43
28. LEED images of 1L O ₂ at 300 K on Cr(110)	45
29. Partial Pressure vs. Temperature curves of various masses for 1L oxygen dosed at room temperature and 1L CO dosed at 120 K on mixed Cr ₂ O ₃ (0001) and Cr(110)	48
30. Partial Pressure vs. Temperature curves for various masses of dosing 1L oxygen and 1L CO 120 K on mixed Cr ₂ O ₃ (0001) and Cr(110)	49
31. Partial Pressure vs. Temperature curves of various masses for 1L oxygen dosed at room temperature and 1L CO dosed at 120 K on Cr(110)	50
32. Partial Pressure vs. Temperature curves of three consecutive dosing of 1L oxygen dosed at room temperature and 1L CO dosed at 120 K on Cr(110)	51

33. Partial Pressure vs. Temperature curves of various masses for 1L oxygen and 1L CO dosed at 120 K on Cr(110)	52
34. Partial Pressure vs. Temperature curves of three consecutive dosing of 1L oxygen and 1L CO dosed at 120 K Cr(110)	53
35. Partial Pressure vs. Temperature curves of 1L CO on Cr(110) and various dosing of co-adsorbed oxygen and CO	54
36. Diagram of sequential dosing of 0.5L CO on Cr(110)	58

ABSTRACT

MEASUREMENT OF THE ADSORPTION KINETICS OF CO AND CO CO-ADSORBED WITH O₂ ON Cr(110)

by

Jennifer L. Walters, BS

Texas State University-San Marcos

May 2010

SUPERVISING PROFESSOR: CARL A. VENTRICE JR.

Previous studies of the adsorption of CO on the catalytically active Cr(110) surface have found that the CO molecule dissociates upon adsorption at 300 K. One aspect of the CO adsorption process that has not been studied in detail is the temperature dependence of the dissociation and the influence of oxygen on the dissociation process. Therefore, we have performed temperature programmed desorption (TPD) and low energy electron diffraction (LEED) measurements of the adsorption of CO and CO co-adsorbed with oxygen on the Cr(110) surface. Deposition of CO was performed at 120 K on either the clean or oxygen dosed Cr(110) surface before performing the TPD

measurements. For deposition below 0.5 Langmuir (L), no CO is detected with TPD, which indicates that all of the CO is dissociating and reacting with the Cr(110) surface. As the CO dose is increased, a broad peak centered at 300 K is first observed, followed by a second peak at 220 K. Oxygen co-adsorption suppresses the dissociation of the CO at low coverages.

CHAPTER I

INTRODUCTION

A. MOTIVATION

The adsorption of carbon monoxide (CO) on single-crystal metal surfaces has been extensively investigated in the past [1]. However, there have been only a few published studies on the adsorption of CO on the catalytically active Cr(110) surface [2]. Since CO is a simple diatomic molecule, it is often used for surface science studies as a model molecule for understanding chemical processes at surfaces. Because the oxidation of CO to form carbon dioxide (CO₂) is an important industrial process, it is of great interest to understand the interaction of CO and oxygen co-adsorbed on catalytically active surfaces such as Cr(110). In this thesis, temperature desorption spectroscopy (TDS) measurements were performed for CO adsorbed on the Cr(110) surface and for CO co-adsorbed with oxygen on the Cr (110) surface. In addition, the surface structure of the clean and adsorbate covered Cr(110) surface were studied using low energy electron diffraction (LEED).

B. PREVIOUS STUDIES

Previous research studies on the adsorption of CO on Cr(110) were done using surface sensitive methods such as electron energy loss spectroscopy (EELS), electron stimulated desorption ion angular distributions (ESDIAD), low energy electron

diffraction (LEED), Auger electron spectroscopy (AES), and high-resolution electron energy loss spectroscopy (HREELS) [2,3]. From these studies CO was found to adsorb onto the clean metal surface in two different molecular bonding modes [4]. These modes are referred to as α_1 CO (laying down phase) and α_2 CO (standing up phase).

CO is found to dissociate at room temperature on chromium [5]. Adsorbing CO on to Cr(110) at 300 K shows no ordered overlayer with LEED [2]. To adsorb molecular CO onto the surface the crystal has to be cooled below 200 K. For CO coverages up to 0.25 monolayer, only the α_1 CO molecules will exist on the surface [2]. Temperature dependent HREELS studies show that the dissociation of the α_1 CO starts at approximately 150 K and is complete by 250 K. At higher coverage a mixed ad-layer of a laying down and standing up phase appears, and desorption of this mixed phase begins around 170 K and finishes around 350 K [3].

A theoretical study has predicted that CO will attach to the surface of Cr (110) in six different bonding sites [6]. The lying down CO is predicted to adsorb preferentially on a short bridge or long bridge binding site, as seen in Figure 1. The standing up CO is predicted to adsorb atop, 2-fold and on the 3-fold sites on the Cr surfaces as shown in both Figure 1 and Figure 2. The 4-fold binding site cannot be considered as a binding site due to the fact that it is too large (chromium atomic spacing is 2.88 Å) for a lying down CO molecule [6]. The 3-fold site is the most stable binding for standing up CO [6]. When O₂ is co-adsorbed with CO on the surface the oxygen takes most of the available bonding sites which leave room for only standing up CO to adsorb.

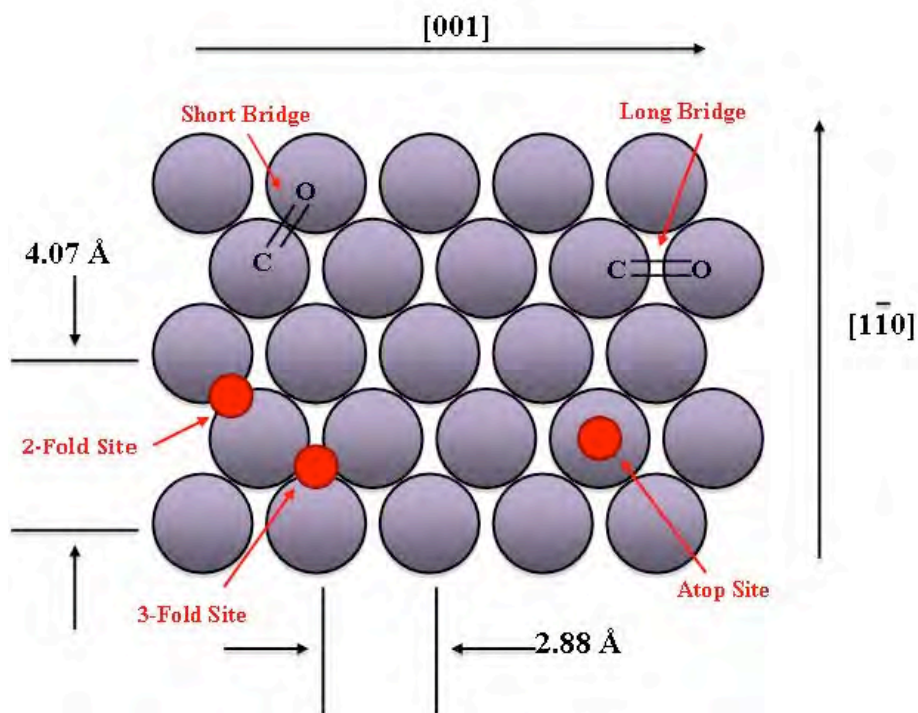


Figure 1: Top view of Cr(110). Primary binding sites for α_1 CO (laying down phase) are the short and long bridge. The 3-fold and atop sites are only occupied by α_2 CO (standing up phase) and are designated by red dots.

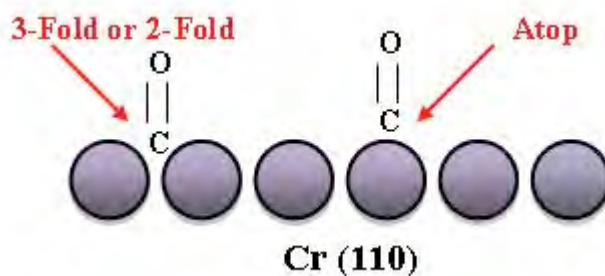


Figure 2: Side view of Cr(110). Only the α_2 CO (standing up phase) are possible for the 3-fold and atop binding sites.

CHAPTER II

INSRUMENTATION AND THEORY

A. ULTRA HIGH VACUUM

Ultra high vacuum (UHV) is established through the use of various pumps attached to a stainless steel chamber. For most modern UHV chambers, the base internal pressure normally falls below $\sim 10^{-10}$ Torr. The UHV chamber for this experiment maintained a base pressure of 3×10^{-11} Torr. Four different pumps were used to achieve this base pressure. The first was a rotary vane pump manufactured by Alcatel Vacuum Products, Inc, with an operating range between atmosphere and a pressure of $\sim 10^{-3}$ Torr. The second pump used was a turbomolecular pump manufactured by Pfeiffer-Vacuum, which can reach a pressure of $\sim 10^{-11}$ Torr. The turbomolecular pump is backed by the rotary vane pump. An ion getter pump and a titanium sublimation pump (TSP), manufactured by Veeco and Varian Vacuum, respectively, were the last two pumps used on this chamber. The ion pump works by ionizing the residual gas molecules in the chamber with field-emitted electrons. These ions are then accelerated into the titanium plates of the ion pump elements, where they react with the titanium. This process is called gettering. In addition, sputtered titanium atoms can trap some non-reactive atoms, such as Argon, during the pumping process. The TSP is used to pump getterable molecules such as nitrogen, water, and hydrogen. The TSP works by passing a current (42 – 45 A) through a filament made of a Ti/Mo alloy, which results in the evaporation of

fresh, unreacted Ti onto the walls of the pump enclosure. This layer of fresh Ti pumps by reacting with molecules that collide with the walls of the pump enclosure. Under typical UHV conditions, the pump is usually flashed once per day [7].

UHV is needed to control the cleanliness of the surface region of samples. From kinetic theory, the impingement rate of molecules striking a surface is given by

$$\dot{n}_s = N_g \sqrt{\frac{RT}{2\pi M}}, \quad (1)$$

where N_g is the number of gas molecules per cm^3 , R is the gas constant, and M is the molecular weight of the molecule [8]. For a monolayer capacity of 3×10^{14} particles/ cm^2 , an average molecular weight of $M = 28$, and $T = 300$ K, the impingement rate is

$$\dot{n}_s \approx 10^6 \cdot p \text{ (monolayers/s)}, \quad (2)$$

where p is the pressure measured in Torr. Therefore, a layer of gas atoms can stick to the surface and change its properties in as little as a second at a pressure of $\sim 10^{-6}$ Torr.

Because of this, gas exposure is commonly measured in Langmuir's, where

$$1 \times 10^{-6} \text{ Torr} \cdot \text{s} = 1 \text{ Langmuir}. \quad (3)$$

The length of time that it takes to form a monolayer of contamination on the surface

depends on the sticking coefficient, s , which is the probability that an impinging molecule is absorbed. This results in

$$\tau \approx \frac{10^{-6}}{s \cdot p}, \quad (4)$$

which is the time it takes to form a monolayer on the surface. Therefore, for a base pressure of 1×10^{-10} Torr (UHV conditions), a surface will remain clean for at least $\tau = 10^4$ s (~3 hours) before surface contamination becomes an issue. For Cr, which is a very reactive surface, the sticking coefficient is very close to one for most residual gasses in the chamber, which means that it is very important to perform surface characterization in UHV.

To achieve UHV, the flanges on the chamber must be sealed with copper gaskets. The knife edges on the connecting flanges plastically deform the copper gaskets once they are tightened down. The system must first be roughed down using a rotary vane pump. Once the chamber reaches $\sim 10^{-3}$ Torr, the turbomolecular pump can be turned on, but this will only bring the pressure down to $\sim 10^{-7}$ Torr since gas molecules adsorbed on the chamber walls before pumpdown will slowly desorb. The chamber then needs to be baked at approximately 150° Celsius for at least twenty-four hours. Baking the chamber removes water and other gasses that are adsorbed on the chamber walls and brings the chamber pressure into the UHV range. Any glass or sensitive instruments are covered with aluminum foil for protection and then the entire system is wrapped in heating blankets to insulate it during the bake out.

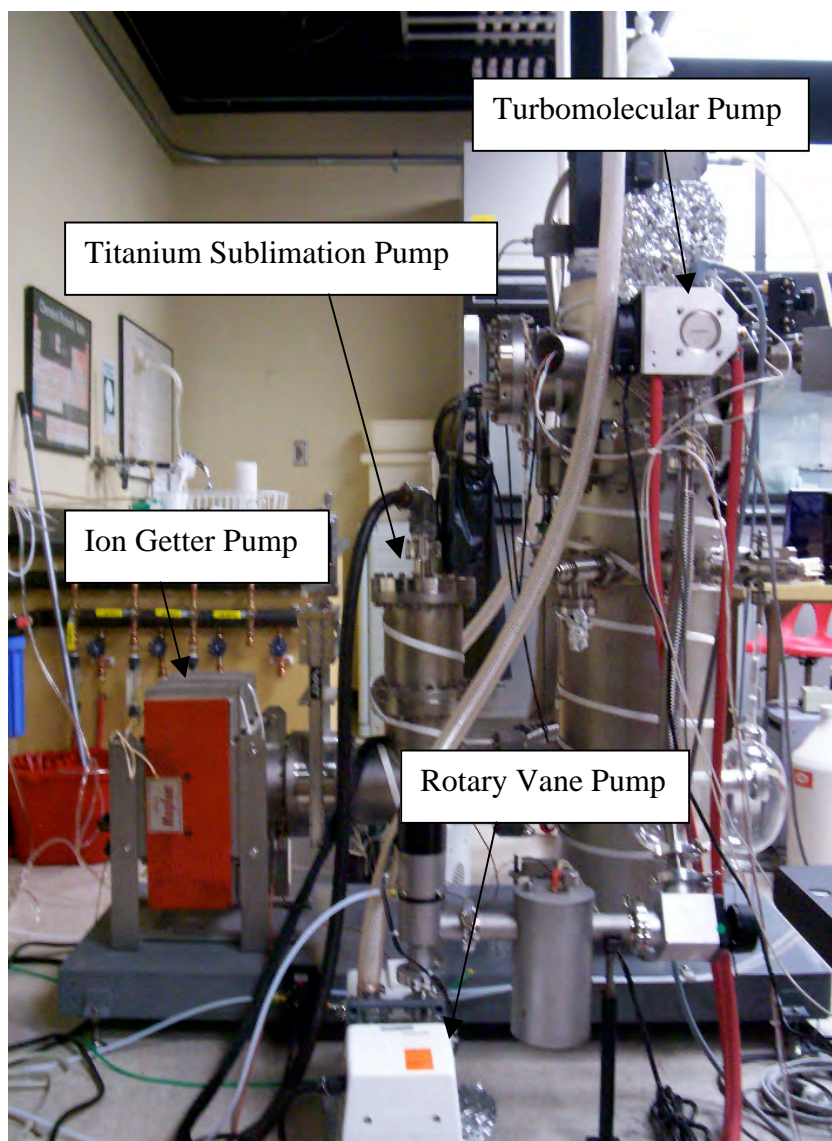


Figure 3: Side view of the experimental chamber showing the various pumps used to achieve UHV. The chamber is wrapped in white heating tape, which is used to bake the chamber.

B. LOW ENERGY ELECTRON DIFFRACTION

The mean free path of electrons in solids is less than ten angstroms over a kinetic energy range of 20 to 500 eV, as shown in Figure 4. Because of this, electrons with kinetic energies in this range can be used to investigate the physical properties of the surface of a solid. One of the most common techniques that are used to determine the crystal structure of surfaces is low energy electron diffraction (LEED) [8].

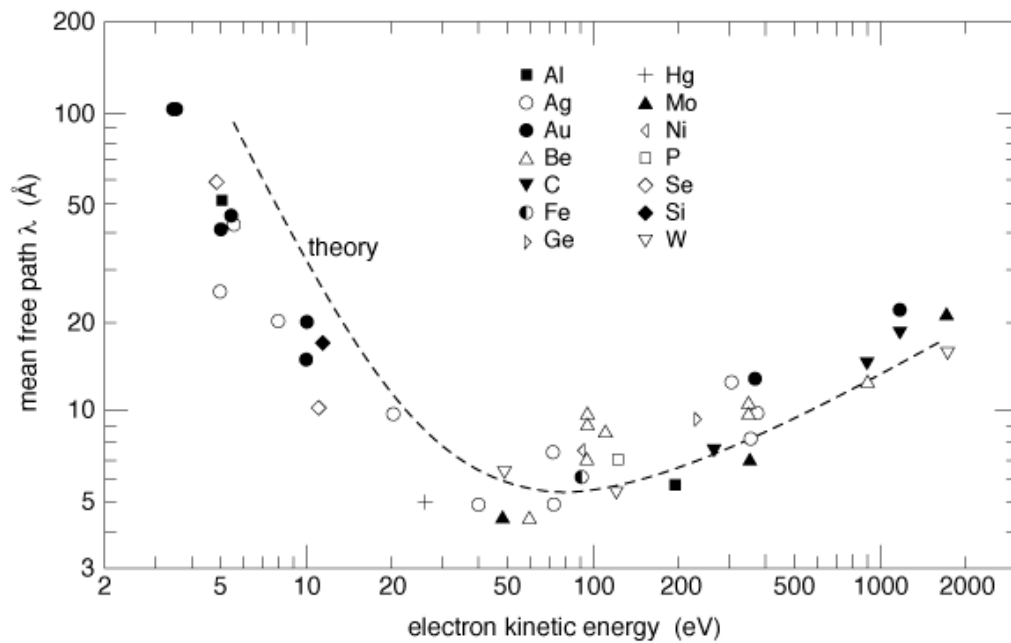


Figure 4: Mean free path of electrons in metallic solids as a function of energy [9].

The first LEED results were published by C.J. Davison and L.H. Germer in 1927 [8]. For most LEED experiments, the incident electron beam is directed normal to the surface of the crystal as shown in Figure 5.

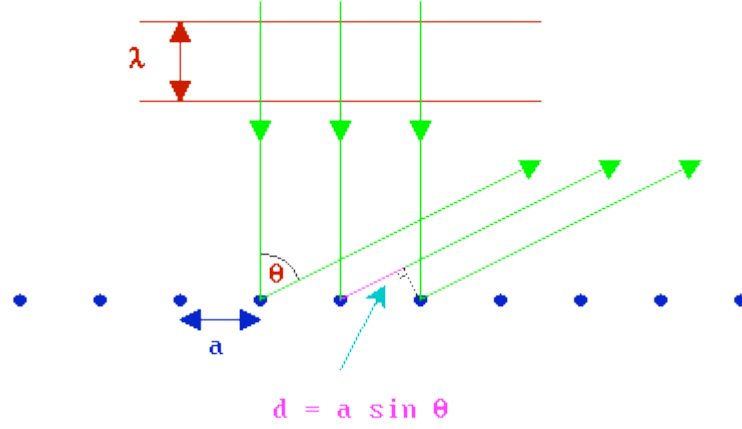


Figure 5: LEED scattering geometry where the path length difference between wavelets from successive atoms is $d = a \cdot \sin \theta$.

For a one dimensional array of atoms, the phase shift of the outgoing electron waves from adjacent atoms separated by distance a is given by

$$d = a \sin \theta . \quad (5)$$

Therefore, the condition for constructive interference of the electron waves is that the phase shift is an integer multiple of the wavelength of the electron,

$$n\lambda = a \sin \theta . \quad (6)$$

The wavelength of the electron is given by the de Broglie relation, [8]

$$\lambda = \frac{h}{mv} = \frac{h}{\sqrt{2mE}} \quad (7)$$

where h is Planck's constant, v is the velocity, m is the mass, and E is the kinetic energy of the electron.

Today, most LEED optics are based on an apparatus developed by J.J. Lander in 1962 [8]. This system consists of hemispherical grids and a phosphorescent screen. The device used for our measurements is a four grid system seen in Figure 6. The first grid (one closest to the sample) is held at ground; this guarantees that there is no electric field between the detector and the sample. The two middle grids are held at a potential energy that is slightly less than the incident beam energy. This allows them to act as a filter, which blocks electrons that have scattered inelastically from the surface from passing to the fourth grid. Just like the first grid, the fourth is also held at ground potential. The phosphorescent screen, or collector, is normally held at a potential between 3 to 5 kV. This results in the emission of light when the electron impacts the phosphor so that the diffraction maxima can be observed. The low energy electrons that impinge on the crystal surface originate from an electron gun located at the center of the hemispherical grid system. A beam ranging between 10-500 eV is directed toward the sample, where the electrons strike normal to the surface and pierce only the first few angstroms of the crystal.

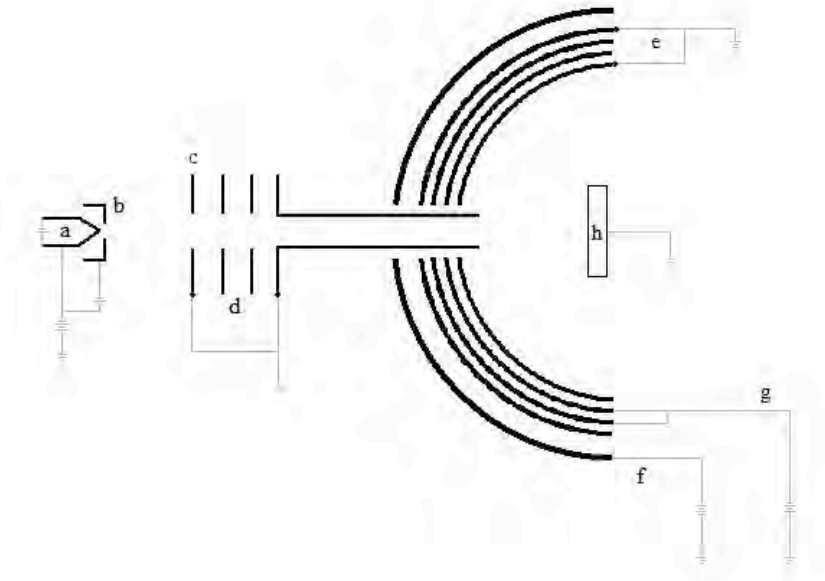


Figure 6: Schematic for an electron gun and four grid LEED detector. (a) filament (b) wehnelt cylinder (c) anode (d) focusing lenses (e) grids 1 and 4 held at ground (f) phosphorescent screen (g) grids 2 and 3 held at a slightly lower potential than the beam energy (h) sample

To understand the information that the LEED pattern gives us, we need to first define what a crystal is and the relationship between the real and reciprocal lattice. A crystal is composed of an atom or group of atoms that repeat in space with the same local symmetry. The arrangement of the atoms is called the basis, and the array formed by repeating the basis is called the lattice. The crystal's lattice can be defined in real space by three primitive vectors ($\mathbf{a}_1, \mathbf{a}_2, \mathbf{a}_3$), so ($\mathbf{x}_1, \mathbf{x}_2, \mathbf{x}_3$) are the primitive vectors of the reciprocal lattice [10]. Positions in the reciprocal lattice are plotted by the set of vectors

$$\mathbf{G} = v_1\mathbf{x}_1 + v_2\mathbf{x}_2 + v_3\mathbf{x}_3, \quad (8)$$

also known as the reciprocal lattice vector, where v_1, v_2, v_3 are integers and

$$\begin{aligned} \mathbf{x}_1 &= 2\pi \frac{\mathbf{a}_2 \times \mathbf{a}_3}{\mathbf{a}_1 \cdot \mathbf{a}_2 \times \mathbf{a}_3} \\ \mathbf{x}_2 &= 2\pi \frac{\mathbf{a}_3 \times \mathbf{a}_1}{\mathbf{a}_1 \cdot \mathbf{a}_2 \times \mathbf{a}_3} \\ \mathbf{x}_3 &= 2\pi \frac{\mathbf{a}_1 \times \mathbf{a}_2}{\mathbf{a}_1 \cdot \mathbf{a}_2 \times \mathbf{a}_3} \end{aligned} \quad (9)$$

Chromium is a body-centered cubic (bcc) structure and has a lattice constant of $a_0 = 2.88$ Å, as shown in Figure 7 [11].

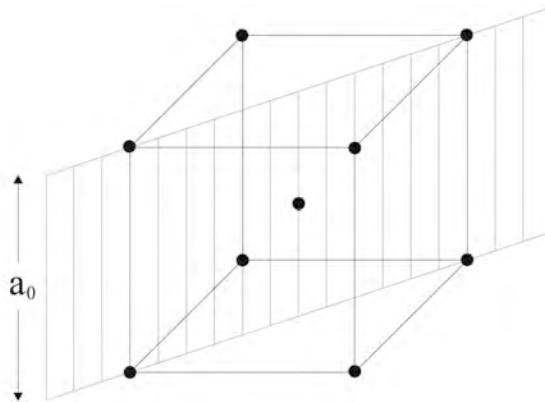


Figure 7: The (110) plane of a bcc conventional cell.

The (110) surface of chromium, which is also called Cr(110), forms a quasi-hexagonal periodic surface with an internal angle of 70.5° , as opposed to 60° for a hexagonal lattice, as shown in Figure 8.

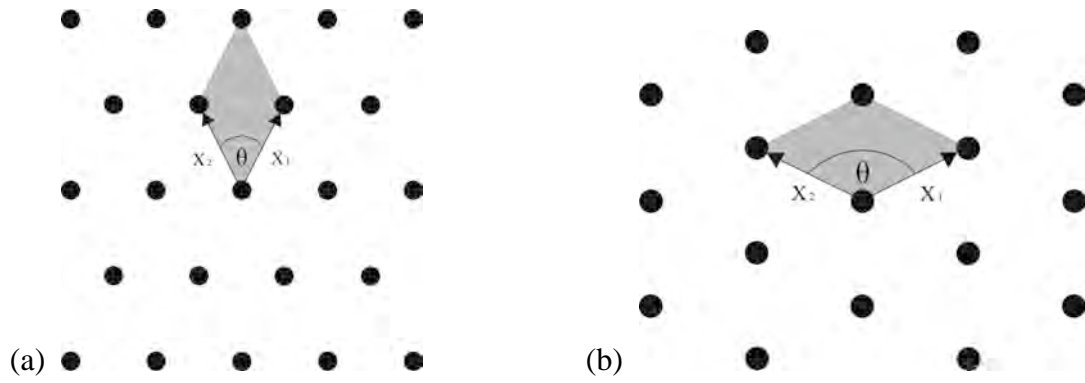


Figure 8: Cr (110) (a) 2-D real space lattice with the primitive cell in grey and (b) 2-D reciprocal lattice with the primitive cell in grey.

The primitive real space lattice vectors of the Cr(110) surface are given by

$$\begin{aligned} \mathbf{x}_1 &= \frac{a_0}{2} \mathbf{i} + \frac{a_0}{\sqrt{2}} \mathbf{j} \\ \mathbf{x}_2 &= -\frac{a_0}{2} \mathbf{i} + \frac{a_0}{\sqrt{2}} \mathbf{j}, \\ \theta &= 70.5^\circ \end{aligned} \tag{10}$$

And the reciprocal space lattice vectors are given by

$$\begin{aligned} \mathbf{x}_1^* &= \frac{2\pi}{a_0} \mathbf{i} + \frac{\sqrt{2}\pi}{a_0} \mathbf{j} \\ \mathbf{x}_2^* &= -\frac{2\pi}{a_0} \mathbf{i} + \frac{\sqrt{2}\pi}{a_0} \mathbf{j}. \\ \theta &= 109.5^\circ \end{aligned} \tag{11}$$

The condition for constructive interference of the electron waves is that the change of wave vector of the electron is equal to a surface reciprocal lattice vector

$$\Delta \mathbf{k} = \mathbf{k} - \mathbf{k}_0 = \mathbf{G}. \quad (12)$$

For LEED measurements, the electrons only probe the first few layers of the surface, and the electron beam is usually incident normal to the surface. Therefore, the condition for constructive interference is

$$\mathbf{k}_{\parallel} = k \sin \theta \hat{\rho} = \mathbf{G}_s, \quad (13)$$

where \mathbf{G}_s is a reciprocal lattice vector of the surface. This result shows that the diffraction pattern observed on the LEED screen is an image of the reciprocal lattice of the surface.

C. QUADRUPOLE MASS SPECTROMETER

A 200 amu quadrupole mass spectrometer (QMS) with electron multiplier was used to measure the partial pressures of each species being released from the surface of the sample. A QMS is also commonly called a residual gas analyzer (RGA). The RGA probe consists of four parallel metal rods with equal but opposite voltage. Ions are accelerated down the length of the space between the rods by an electric field as seen in Figure 9. Two of the rods have an applied potential of $-(U+V\cos(\omega t))$ and the two

opposite have an applied potential of $(U + V \cos(\omega t))$. U denotes the DC voltage while $V \cos(\omega t)$ denotes the AC voltage [12]. The voltage is varied by a radio frequency (RF) oscillation, which only allows resonant ions to pass down the length of the rods. The QMS is mounted on a linear translator that allows it to be moved within a few millimeters of the sample.

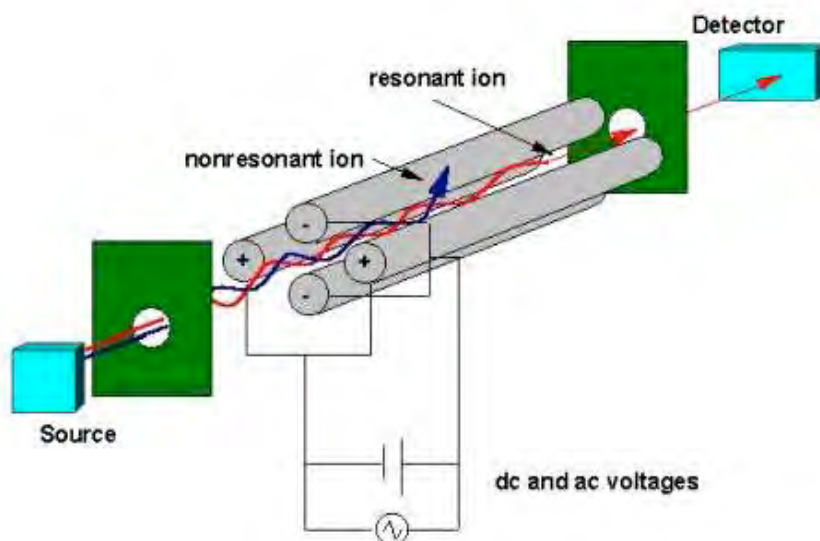


Figure 9: Quadrupole Mass Spectrometer schematics [13]. Only ions of a certain mass to charge ratio (m/z) will reach the detector.

A Hiden Analytical QMS, HAL 201 was used to send and receive signals by way of the RS232 ports located on the interface unit (IU) and the computer. The IU has five LED's that denote whether the QMS is running, which of the two filaments are being used, if the required emission was obtained, and if any internal defaults were detected.

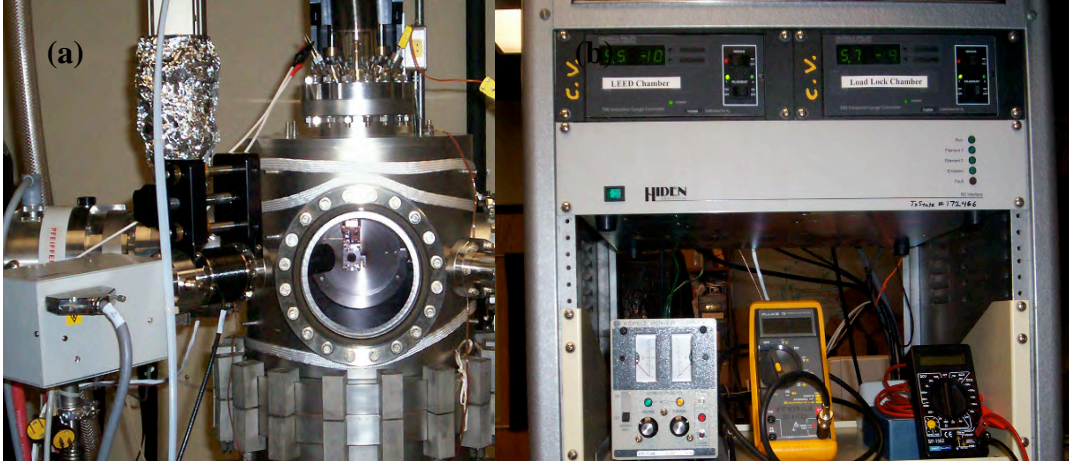


Figure 10: Quadrupole Mass Spectrometer and Hidden Interface Unit. (a) Quadrupole Mass Spectrometer (b) Hidden Interface Unit

D. SAMPLE HOLDER

A sample holder is attached to the chamber via an x-y-z manipulator with a differentially pumped rotary motion feed-through. It is fixed to the bottom of a dewar, where air can be blown in to prevent the sample holder from overheating during a hot sputter or during the annealing process. Figure 11 shows where liquid nitrogen (LN₂) can also be added to the dewar to cool the sample to 120 K.

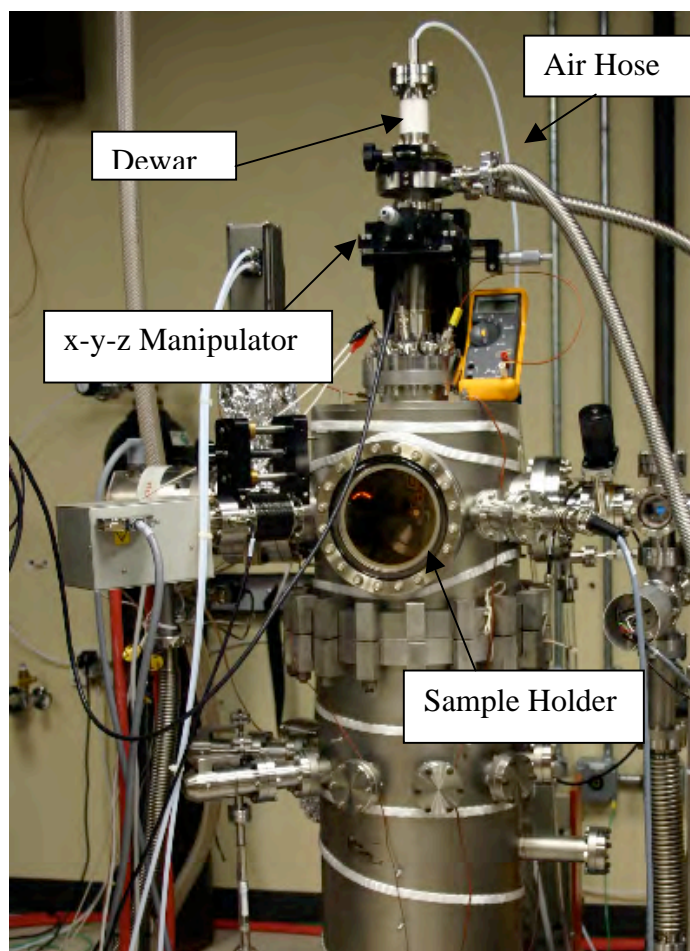


Figure 11: Front view of the experimental chamber.

Two tantalum wires were spot welded to the crystal and the wires were spot welded to a molybdenum plate that was attached to the sample holder at the end of the dewar assembly. A thermocouple was spot welded to the side of the crystal to allow measurement of the temperature of the sample, seen in Figure 12. By amplifying the signal from the thermocouple with a preamp, the temperature could be read by the computer using a data acquisition (DAQ) board. The voltage from the thermocouple can be converted to a temperature by

$$T = \sum_{n=0}^N a_n v^n, \quad (14)$$

where a is a coefficient and n can vary from 0 to 9. The n value also depends on the type of thermocouple used. In this experiment, a chromel-alumel or type k was used. The values for a_n are only valid over a finite temperature range. For our experiment, two lookup tables were used for the temperature conversion: one for -200 °C to 0 °C and a second from 0 °C to 500 °C, as seen in Table 1.

Through radiative heating from a tungsten filament attached to the back of the sample, the temperature can be increased. The filament current is produced by an ATE 15-6M KEPCO power supply. The program used to control the temperature ramp was written by Nicolas Clark [14].

Table 1: Polynomial Coefficients for a type K thermocouple

n	a_0 (-200 to 0 °C)	a_0 (0 to 500 °C)
0	0.00	0.00
1	2.517×10^{-2}	2.508×10^{-2}
2	-1.166×10^{-6}	7.860×10^{-8}
3	-1.083×10^{-9}	-2.503×10^{-10}
4	-8.977×10^{-13}	8.315×10^{-14}
5	-3.734×10^{-16}	-1.228×10^{-17}
6	-8.663×10^{-20}	9.804×10^{-22}
7	-1.045×10^{-23}	-4.413×10^{-26}
8	-5.192×10^{-28}	1.057×10^{-30}
9	n/a	-1.052×10^{-35}
Error Range	0.04 to -0.02 °C	0.04 to -0.05 °C

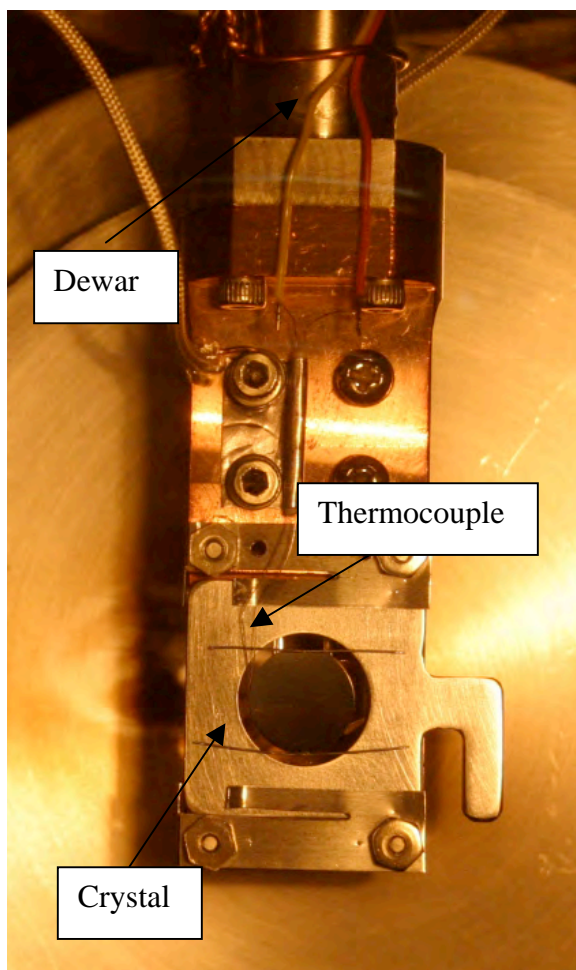


Figure 12: Sample holder assembly with Cr(110) sample crystal. The Thermocouple is touching the crystal so that the actual sample temperature can be read.

E. TEMPERATURE PROGRAMMED DESORPTION

Temperature programmed desorption (TPD), which is also referred to as thermal desorption spectroscopy (TDS), is a technique widely used to study the desorption kinetics of molecules from the surface of materials. Once the sample has been exposed to

the adsorbing molecules, it is placed in front of the QMS. A linear temperature ramp is applied to the sample as expressed in equation (15),

$$T_s = T_0 + \beta t \quad (15)$$

where T_s is the sample temperature, T_0 is the initial temperature and β is the heating rate [13].

To relate the pressure rise measured by the QMS to the desorption rate from the surface of the crystal, an analysis of the sources of gasses in the chamber and the pressure measurement process is needed. In a chamber of volume V , molecules with density c_g desorb from the walls at rate L and are removed by vacuum pumps at a pumping speed S . There are also gas molecules desorbing from the surface of the crystal, which has area A_s . The rate of desorption of the gas molecules from the surface is given by $r_{des}(t)$. The total number of gas-phase molecules can be found by

$$V \frac{dc_g}{dt} = A_s r_{des}(t) + L - c_g S. \quad (16)$$

If the sample holder does not increase in temperature as the crystal is heated, L and S can be considered constant. At the initial temperature, no desorption should take place on the sample, and the gas phase attains a steady-state composition given by

$$V \frac{dc_g}{dt} = L - c_g S = 0. \quad (17)$$

The steady-state solution is

$$c_{gs} = \frac{L}{S}, \quad (18)$$

which corresponds to a steady-state pressure of

$$p_s = k_B T_g c_g = \frac{k_B T_g L}{S}. \quad (19)$$

The pressure change caused by desorption is

$$\Delta p = p - p_s. \quad (20)$$

The relationship between the pressure change and the rate of desorption is

$$V \frac{d\Delta p}{dt} + S\Delta p = k T_g A_s r_{des}(t). \quad (21)$$

In the limit of high pumping speed

$$\Delta p = \frac{k_B T_g A_s}{S} r_{des}(t). \quad (22)$$

This means the desorption rate and the measured pressure change are directly proportional, and the shape and position of the desorption peak holds information about the kinetics [13].

The kinetic parameters governing the reaction can be found by applying the Polanyi-Wigner formula

$$r_{des} = -\frac{\partial \theta}{\partial t} = v_n \theta^n \exp\left(-\frac{E_{des}}{RT_s}\right), \quad (23)$$

where v_n is the pre-exponential factor of the chemical process of order n , T_s is the surface temperature, and E_{des} is the desorption activation energy. Assuming that v_n and E_{des} are independent of coverage and if a linear temperature ramp is substituted into equation (23), the first-order desorption is found to be

$$\frac{E_{des}}{RT_p^2} = \frac{v}{\beta} \exp\left(\frac{-E_{des}}{RT_p}\right) \quad (24)$$

and for the second-desorption

$$\frac{E_{des}}{RT_p^2} = \frac{2v^2}{\beta} \theta_p \exp\left(\frac{-E_{des}}{RT_p}\right) \quad (25)$$

where θ_p is the coverage at T_p . Looking at the peak shape can also give information about the desorption. As coverage drops during the experiment, the desorption order changes, which creates a peak. First-order desorption leads to symmetric peaks and second-order desorption leads to asymmetric peaks [13].

F. SAMPLE PREPARATION TECHNIQUE

To clean the surface of the chromium crystal, it is sputtered using inert gas ions. For our measurements, argon was used as the sputter gas. The first step in this process is to close the gate valves to the ion pump and the turbo pump and backfill the UHV chamber to $P = 5 \times 10^{-5}$ Torr with Ar. A variable leak valve is used to control the amount of Ar backfilled into the chamber. The crystal must be positioned in front of the ion gun so that once the atoms are ionized and accelerated through a potential, they will collide with the surface to remove impurities, as shown in Figure 13. This process is called sputtering. There were two kinds of sputtering techniques used in this experiment, cold sputter and hot sputter. Since a new Cr crystal typically has a lot of nitrogen and carbon impurities in the bulk, hot sputtering is used during the first several sputter cycles to increase the rate of impurity diffusion to the surface of the crystal. Although sputtering removes the unwanted atoms on the surface, the process also damages or disorders the surface of the crystal. To heal the surface the sample must be annealed to give the atoms enough mobility to re-order the surface of the crystal.

To clean the crystal using a cold sputter, the chamber is backfilled with argon to a pressure of 5×10^{-5} Torr. The ions are then accelerated through a potential of 1 kV for 30 minutes at room temperature. The sample is then annealed by the process of electron-beam heating. This is achieved by heating the filament attached to the backside of the sample and biasing the sample at 750 V to accelerate the electrons from the hot filament into the back of the crystal. A type K (chromel/alumel) thermocouple spot welded to the edge of the crystal was used to monitor the temperature during the process. The sample is heated to $\sim 1000\text{K}$ for 5 minutes.

For a hot sputter the chamber is again backfilled with argon to a pressure of 5×10^{-5} Torr. The sample is heated by radiative heating from the filament attached to the back of the crystal, to approximately 870 K. Once the sample is hot, ions were then accelerated through a potential of 1 kV for 1 hour. Again, the surface needs to be healed. The same process for the electron-beam heating used after the cold sputter can be used here.

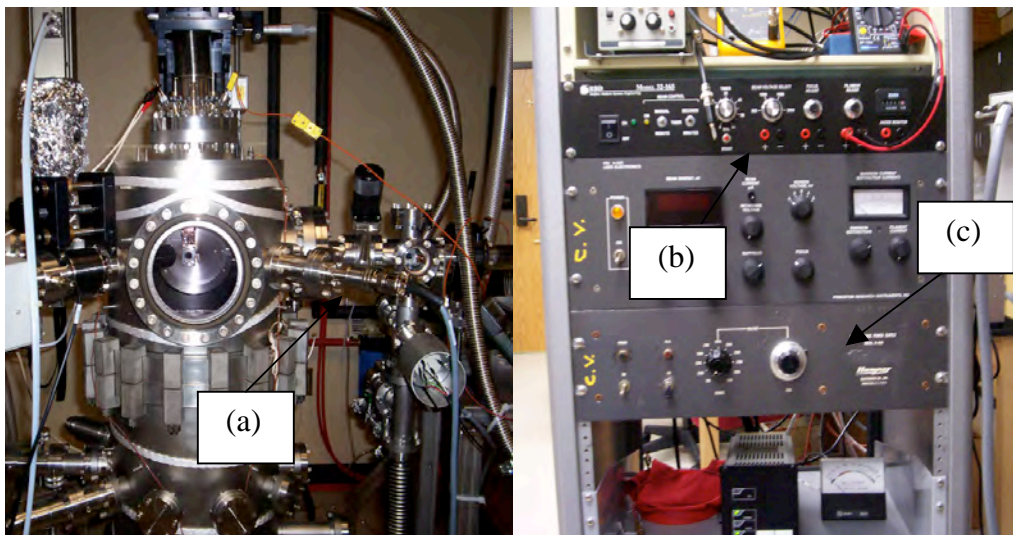


Figure 13: Front of the experimental chamber and Control Rack. (a) Ion Gun (b) Sputter controls (c) High Voltage

For CO to adsorb on to the surface of Chromium, it first needs to be cooled to at least -150°C [2]. To do this, liquid nitrogen was pored down the dewar to cool the sample. Once the sample reached a temperature between -155°C and -160°C , a leak valve was used to dose CO, CO_2 , or oxygen on the surface of the sample, shown in Figure 14. The dosing rates were measured in Langmuirs, as shown in equation (3). Once dosing was complete, TPD measurements were made at a heating rate of $50^{\circ}\text{C}/\text{min}$ and a max temperature of 200°C .

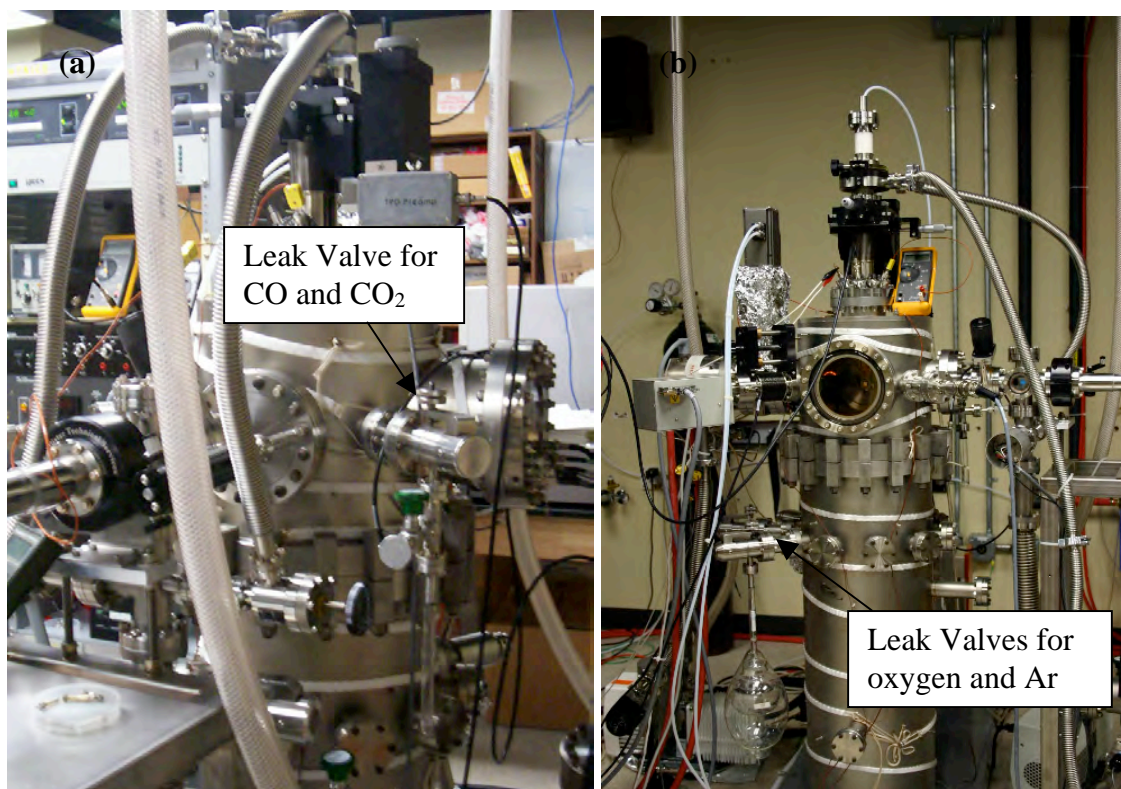


Figure 14: (a) The back side of the UHV chamber where the leak valve is located to bleed in CO and CO_2 for dosing the crystal surface. (b) The front of the UHV chamber where the leak valve for oxygen dosing is located, as well as the leak valve for argon (used in sputtering).

CHAPTER III

RESULTS

A. ADSORPTION OF CO ON MIXED $\text{Cr}_2\text{O}_3(0001)$ AND $\text{Cr}(110)$

Prior to the measurements of CO adsorption on $\text{Cr}(110)$, a study was performed by another graduate student in our group, Gabriel Arellano, on the adsorption of CO on an epitaxial film of $\text{Cr}_2\text{O}_3(0001)$ grown on a $\text{Cr}(110)$ crystal. Since the same $\text{Cr}(110)$ crystal was used for the adsorption measurements presented in this thesis project, the first step was to prepare a clean $\text{Cr}(110)$ surface. After one sputter anneal cycle, the hexagonal LEED pattern of the $\text{Cr}_2\text{O}_3(0001)$ surface became very faint and the quasi-hexagonal pattern of $\text{Cr}(110)$ could be observed, as seen in Figure 15b. However, it also can be seen that the LEED pattern of the $\text{Cr}(110)$ surface had streaks due to the presence of surface impurities, primarily nitrogen and carbon, that had segregated from the bulk of the crystal. To remove the bulk impurities, the crystal was sputtered and annealed twice more to prepare a $\text{Cr}(110)$ surface that was free of impurities, as seen in Figure 15c.

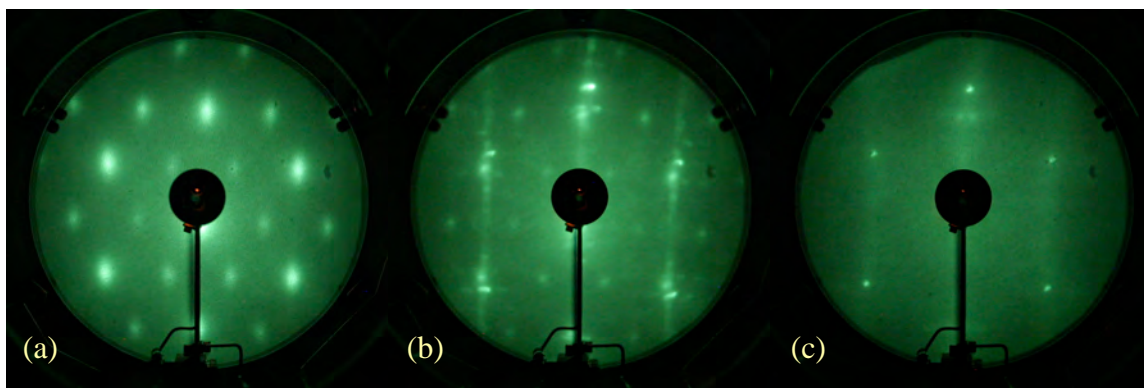


Figure 15: LEED images at 75 eV of (a) the $\text{Cr}_2\text{O}_3(0001)/\text{Cr}(110)$ surface, (b) the $\text{Cr}(110)$ surface after one sputter-anneal cycle, where the pattern from some residual $\text{Cr}_2\text{O}_3(0001)$ can be seen, and (c) the clean $\text{Cr}(110)$ surface.

The initial carbon monoxide TPD measurements were performed after three sputter-anneal cycles since the LEED images indicated no sign of residual Cr_2O_3 on the surface. However, the TPD spectra showed a distinct peak at the same temperature that was observed for CO desorption from the $\text{Cr}_2\text{O}_3(0001)/\text{Cr}(110)$ surface. This indicates that the Cr_2O_3 was not completely removed from the surface. A comparison of TPD spectra for 1 L of CO adsorbed on $\text{Cr}_2\text{O}_3(0001)/\text{Cr}(110)$, the $\text{Cr}(110)$ surface after three sputter-anneal cycles, and the clean $\text{Cr}(110)$ surface after several weeks of daily sputter-anneal cycles are shown in Figure 16. For the $\text{Cr}_2\text{O}_3(0001)/\text{Cr}(110)$ surface, a large peak is seen at 175 K. The spectrum taken after three sputter-anneal cycles shows a small peak at 175 K and broad peaks at 210 K and 290 K. Whereas, the spectrum taken after several sputter-anneal cycles were performed shows only the two broad peaks, without the peak at 175 K.

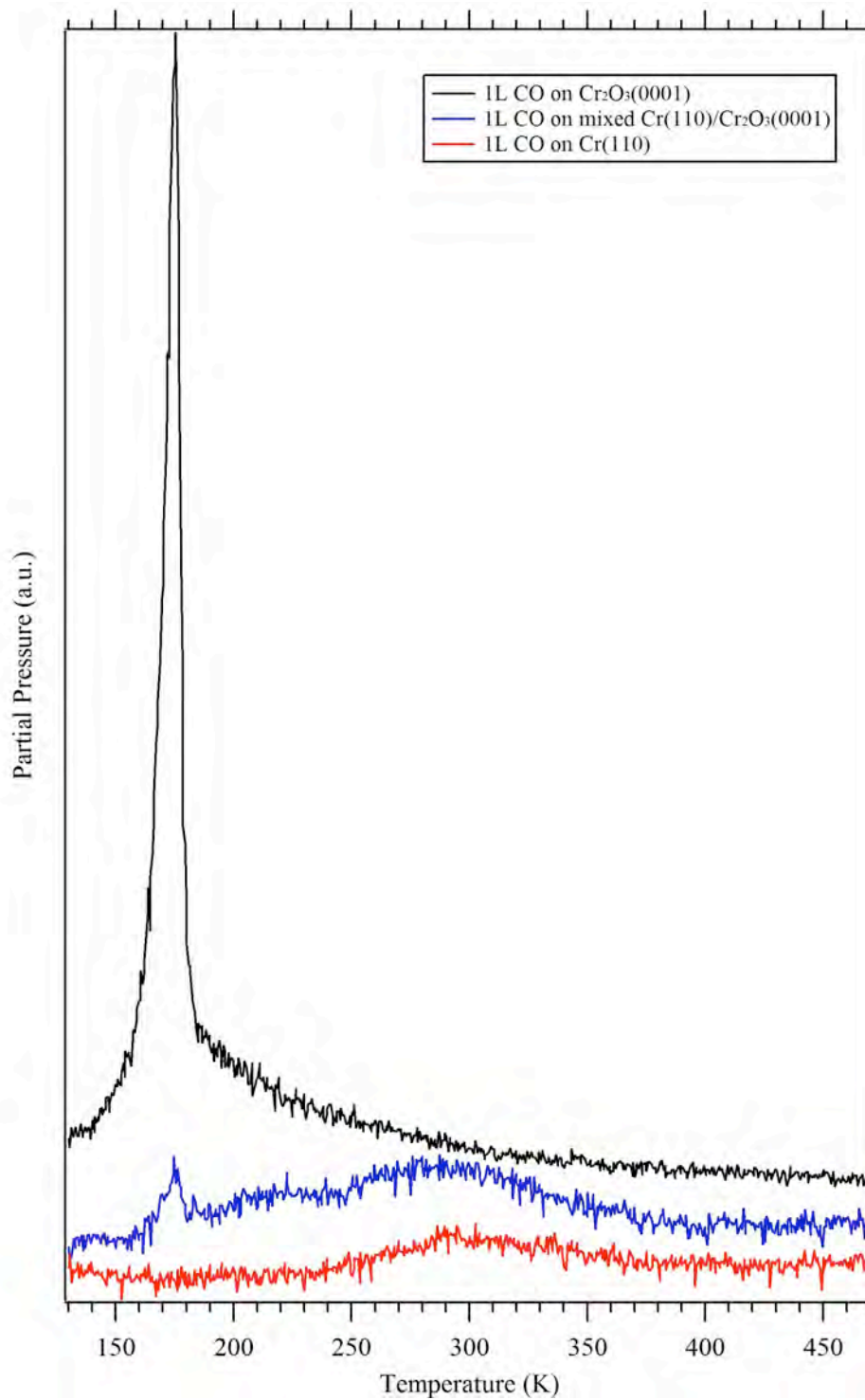


Figure 16: Partial pressure versus temperature curve of CO on different substrates. All spectra were taken at a heating rate of 50°C/min and are offset for clarity.

A dosing sequence for CO adsorbed on the mixed $\text{Cr}_2\text{O}_3(0001)$ and $\text{Cr}(110)$ surface is shown in Figure 17. In this experiment, the surface was dosed with 0.5 L followed by a TPD measurement, and this sequence was then repeated for doses of 1.0 L, 5 L, and 10 L. All four spectra show the same peak at 175 K with the same peak height as was observed previously in Figure 16 for the mixed phase surface. It is noted that the surface was not sputtered and annealed between subsequent CO adsorptions. For the 0.5 L adsorption, two broad peaks are observed at 210 K and 300 K. For the higher CO doses, the peak at 210 K increases, whereas, the higher binding energy peak at 300 K remains at about the same intensity.

To determine if molecular species other than CO were desorbing from the mixed phase surface, several masses were measured during the TPD measurements, as shown in Figure 18 for a dose of 1.0 L of CO. The masses that were monitored with the corresponding chemical composition are 12 (C), 15 (CH_3), 18 (H_2O), 28 (CO), 32 (O_2), and 44 (CO_2). The only measured mass that gives a large peak is mass 28 (CO). However, a slight peak is also observed for mass 12 (C) since it is a cracking fragment of CO with an expected intensity of 5% of the CO intensity.

To determine the effect of dosing the surface without intermediate sputter-anneal cycles, the spectra for three subsequent doses of 1.0 L of CO are shown in Figure 19. It can be seen in this figure that the area under the pressure versus temperature curve for the first dose is much less than for the second and third doses. The relative peak height of the 210 K and 300 K peaks also changes between the first and the second or third doses. This result provides evidence that the initial coverage of CO does not completely desorb from the surface during the TPD measurement.

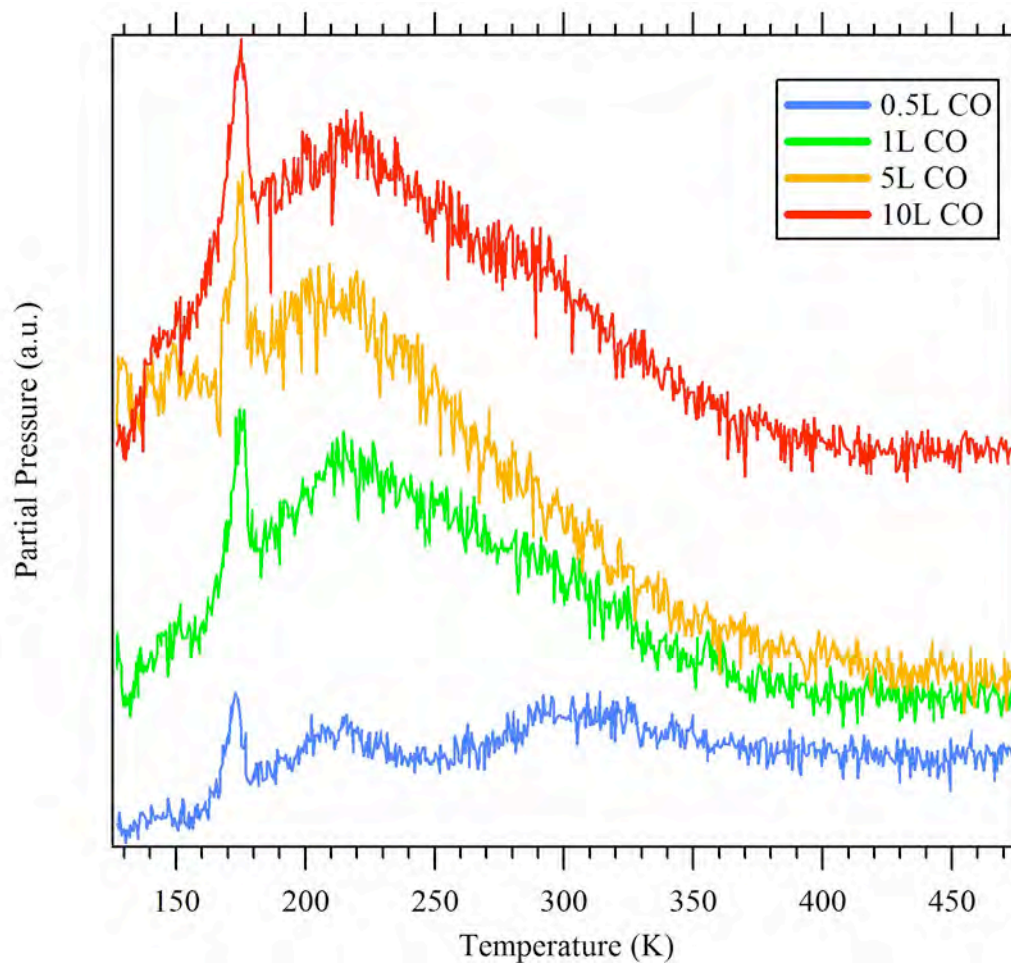


Figure 17: Partial pressure versus temperature curve for four consecutive dosing of CO on mixed $\text{Cr}_2\text{O}_3(0001)$ and $\text{Cr}(110)$. All spectra were taken at a heating rate of $50^\circ\text{C}/\text{min}$ and are offset for clarity.

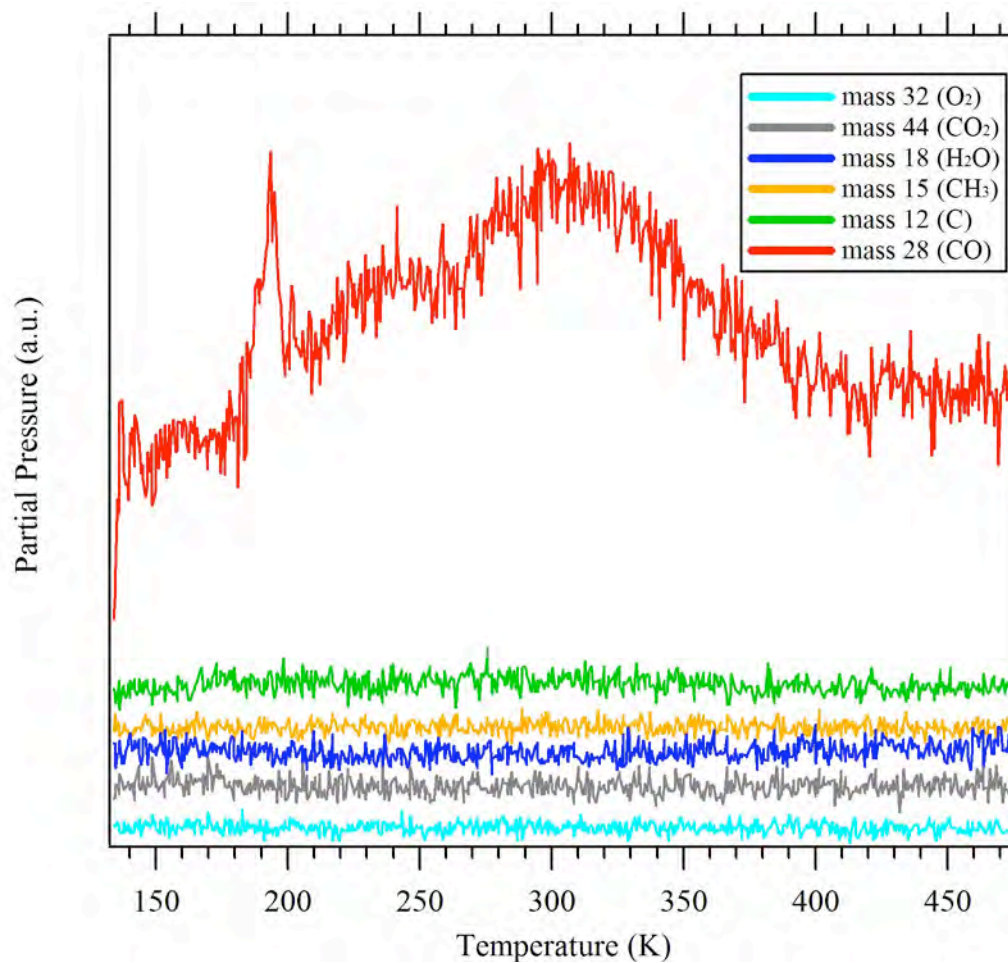


Figure 18: Partial pressure versus temperature curve of various masses measured for 1L dosing of CO on mixed $Cr_2O_3(0001)$ and $Cr(110)$. All spectra were taken at a heating rate of $50^\circ C/min$ and are offset for clarity.

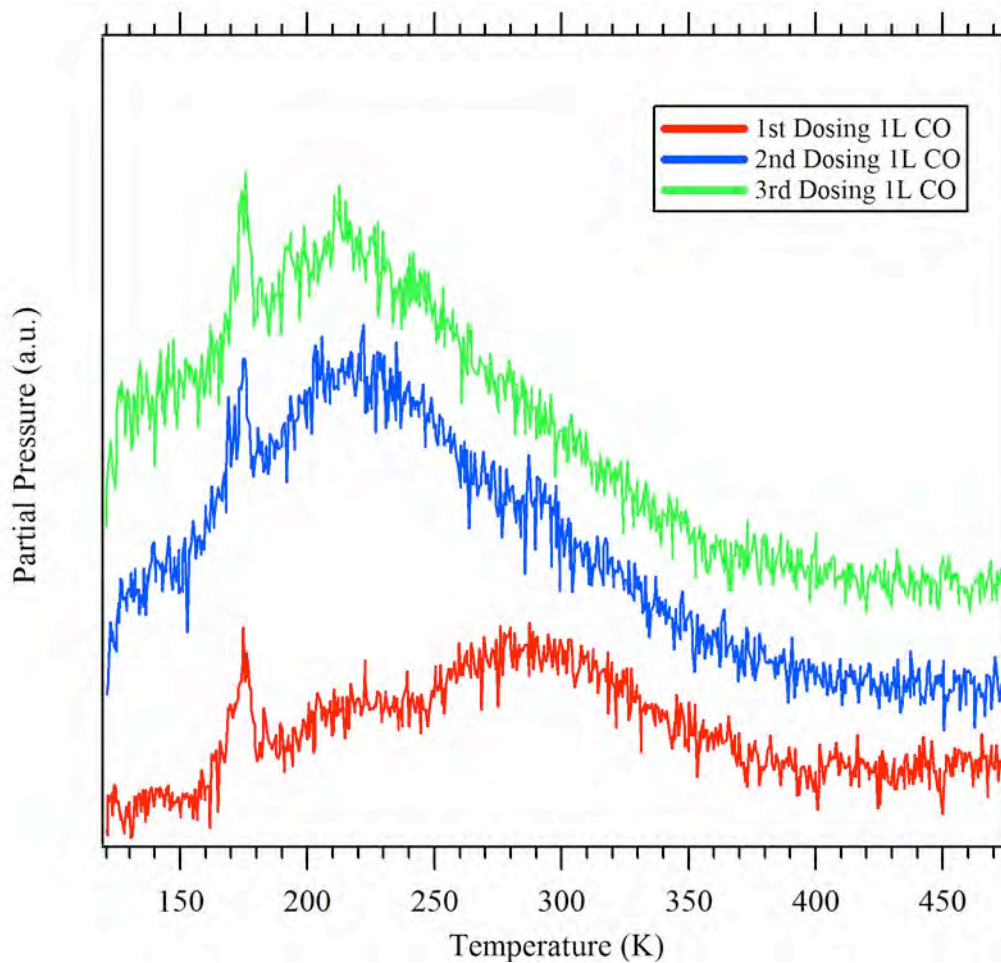


Figure 19: Partial pressure versus temperature curve of three consecutive dosing of 1L CO on mixed $\text{Cr}_2\text{O}_3(0001)$ and $\text{Cr}(110)$. All spectra were taken at a heating rate of $50^\circ\text{C}/\text{min}$ and are offset for clarity.

B. ADSORPTION OF CO ON Cr (110)

The sample was cleaned by daily cycles of hot sputtering with Ar and annealing in UHV over a period of about six weeks to remove any residual chrome oxide on the surface and to reduce the presence of bulk impurities of nitrogen and carbon that will diffuse to the surface during the UHV anneal [15]. Once the sputter/anneal process was complete LEED was performed to investigate the cleanliness of the surface. The quasi-hexagonal structure of Cr(110) can still be seen in Figure 20, as well as some extra faint spots. All of the oxide on the surface has been removed, but some nitrogen, and possibly some carbon still seem to remain. Normally, precipitated carbon on the surface is expected to form a ring pattern due to the presence of randomly oriented graphite crystallites on the surface. Since this feature is missing from all of the LEED photos, we can assume that at most only a small amount of carbon is left on the sample. Nitrogen contamination in Cr is common and forms a long-range herringbone style surface reconstruction [15]. Therefore, we feel that there is probably a slight amount of nitrogen contamination on the surface. The goal was to achieve a pristine surface, but this would have taken several more months of hot sputter/anneal cycles.

The adsorption geometry of CO on the Cr(110) surface was monitored using LEED. For a dose of 1.0 L of CO, the LEED patterns showed no extra spots and only a slight increase in diffuse background, as shown in Figure 21. This result indicates that the CO that is adsorbed on the surface is either forming a (1x1) overlayer or is completely disordered so that the quasi-hexagonal spots that are observed are only from the Cr(110) substrate atoms.

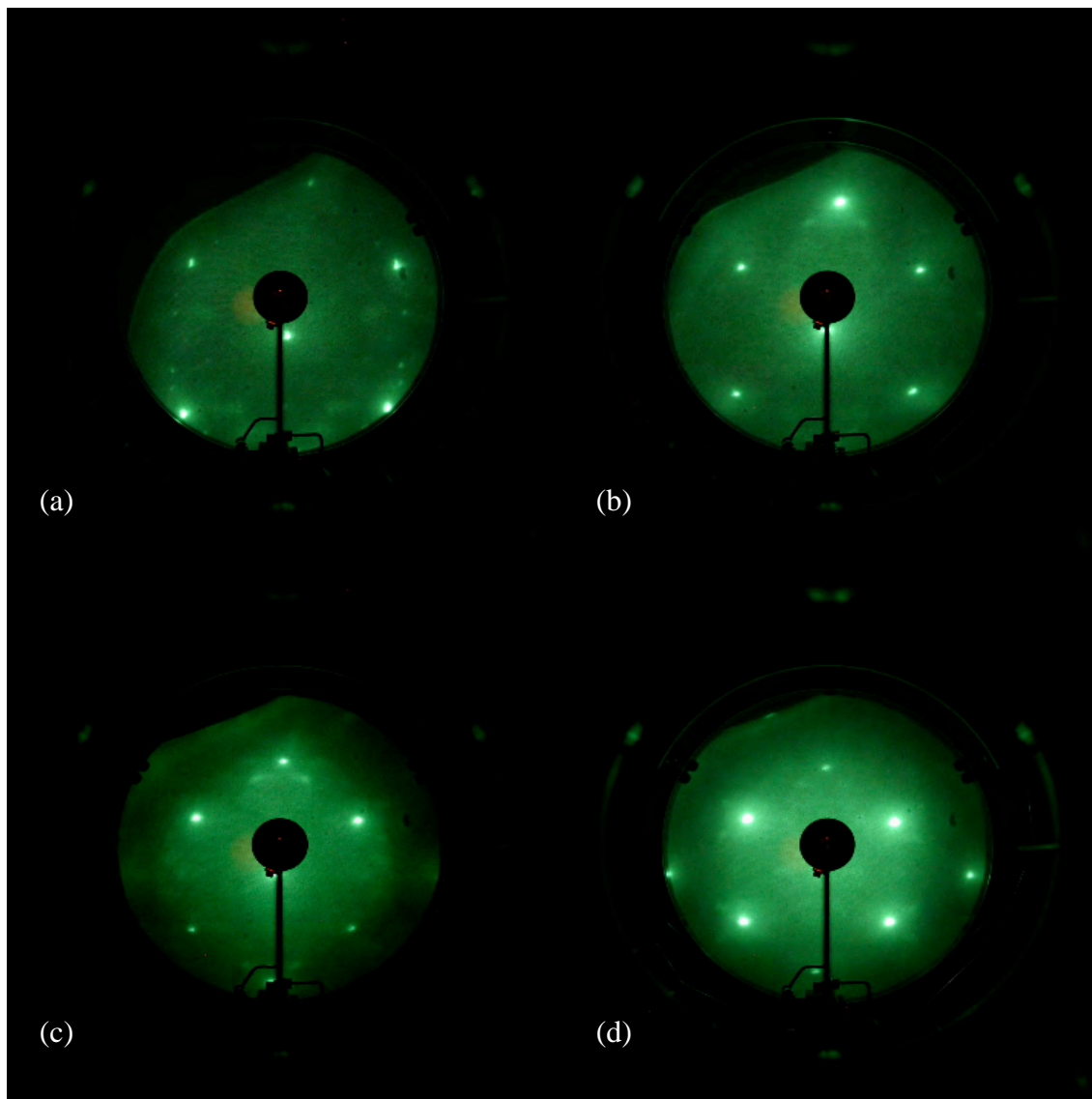


Figure 20: LEED patterns of Cr(110) after twenty-two hot sputter/anneal cycles. Beam energies: a) 54.6eV, b) 75.1eV, c) 95.4eV, d) 112.8eV

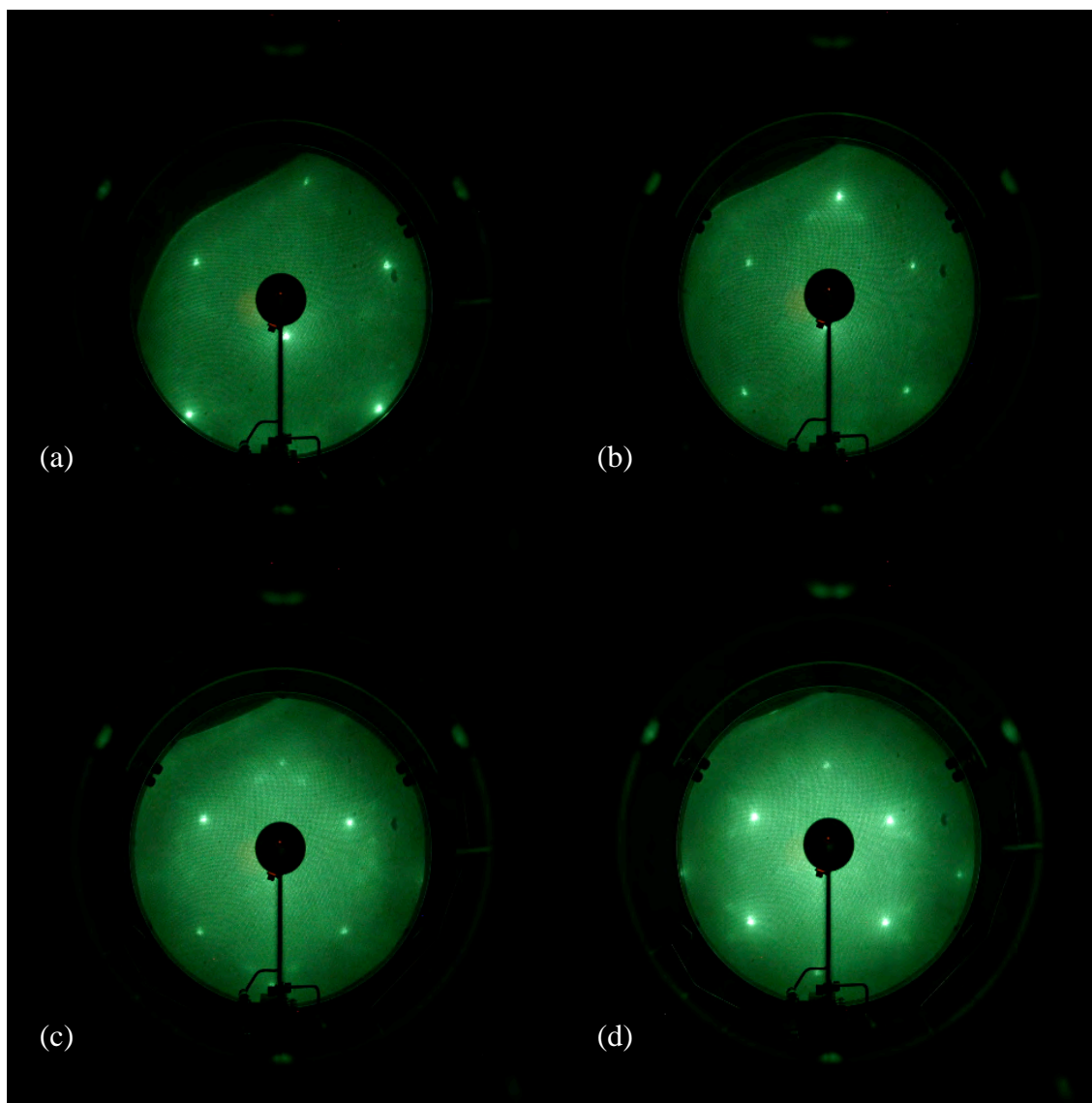


Figure 21: LEED patterns of Cr(110) with 1L of CO dosed at room temperature on the surface after twenty-two hot sputter/anneal cycles. Beam energies: a) 54.6 eV, b) 75.1 eV, c) 95.4 eV, d) 112.8 eV

After the sample was declared clean enough for the CO adsorption measurements, a series of TPD studies were conducted. To determine the molecular species desorbing from the surface, TPD spectra from masses 12 (C), 15 (CH₃), 18 (H₂O), 28 (CO), 32 (O₂), and 44 (CO₂) after 1 L of CO was adsorbed on the surface are shown in Figure 22. As with the mixed surface phase, only mass 28 (CO) shows a peak. There are two peaks observed: one peak at 200 K and a second peak at 300 K. However, the 200K peak is much smaller than the 300 K peak; whereas, both peaks were of similar size for the mixed surface spectra.

The TPD spectra for four consecutive adsorptions of 0.5L of CO, without performing sputter-anneal cycles between the CO doses, are shown in Figure 23. The TPD spectrum taken after the first 0.5 L adsorption shows almost no CO signal, only a very small peak at 320 K. The second dose (completed without an intermediate sputter-anneal cycle) results in a single much larger peak at 300 K, which is shifted 20 K lower than the first dose. It is noted that the spectrum for second dose of 0.5 L CO looks similar to the spectrum for the dose of 1L CO shown in Figure 22. The third and fourth doses were also completed without intermediate sputter-anneal cycles in between runs. Both of these spectra have two peaks and are shifted to a lower temperature as compared to the two earlier runs. These peaks are located at 260 K and 290 K.

The TPD spectra for three successive adsorptions of 1 L of CO on Cr(110) is shown in Figure 24. The TPD spectrum after the first adsorption of 1 L is similar to the 1 L CO dose shown in Figure 22, where a peak is seen at 200 K and 300 K. It is also similar to the spectrum of two consecutive 0.5 L adsorptions shown in Figure 23. The second and third adsorptions of 1 L were done without performing an intermediate

sputter-anneal cycle and show a single large peak at 230 K. This main peak has shifted 70 K lower than the main peak for the first adsorption of 1 L.

The same procedure was done for three consecutive adsorptions of 5L CO and 10L CO. The results for 5L CO adsorptions on Cr(110) are shown in Figure 25. The first dosing shows two peaks, one at 225 K and one at 285 K. The second and third measurements have much less defined peaks but, the peak positions are the same as the first dosing. The results for 10 L CO adsorptions on Cr(110) are shown in Figure 26. The TPD spectra for this set of measurements are similar to those shown in Figure 25. All spectra have two peaks located at 225 K and 285 K.

The first dosing of 0.5 L, 1 L, 5 L, and 10 L of CO on Cr(110) are compared in Figure 27. In other words, all these spectra are for adsorption of CO on a freshly sputtered and annealed Cr(110) surface. At low coverage (0.5 L), a very small peak is seen at 320K. As the amount of CO adsorbed increases, the peaks shift left to lower temperatures. For 1 L of CO, the peak has shifted 30 K lower than 0.5 L. The spectrum for the fourth dosing of 0.5 L CO (from Figure 23) was also graphed for comparison and is nominally equivalent to a dosing of 2L CO. This measurement reveals two peaks, one at 260 K and 290 K. The measurements for 5L CO and 10L CO both have a peak at 285 K, which is positioned almost exactly where one of the peaks for the fourth dosing of 0.5 L is located. The second peak for both of these measurements is positioned at 225 K. This peak has shifted 35 K lower than the second peak seen for the fourth dosing of 0.5 L of CO.

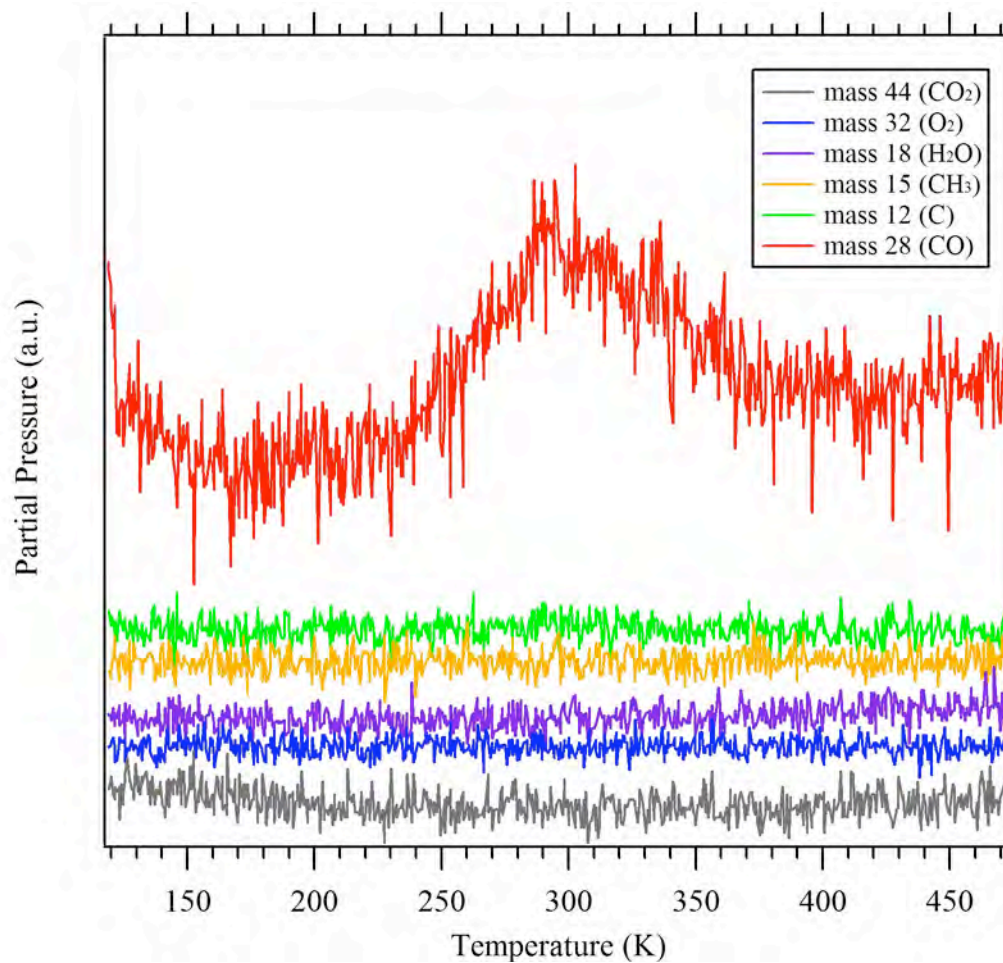


Figure 22: Partial pressure versus temperature curves of various masses for dosing 1L CO on Cr(110). All spectra were taken at a heating rate of 50°C/min and are offset for clarity.

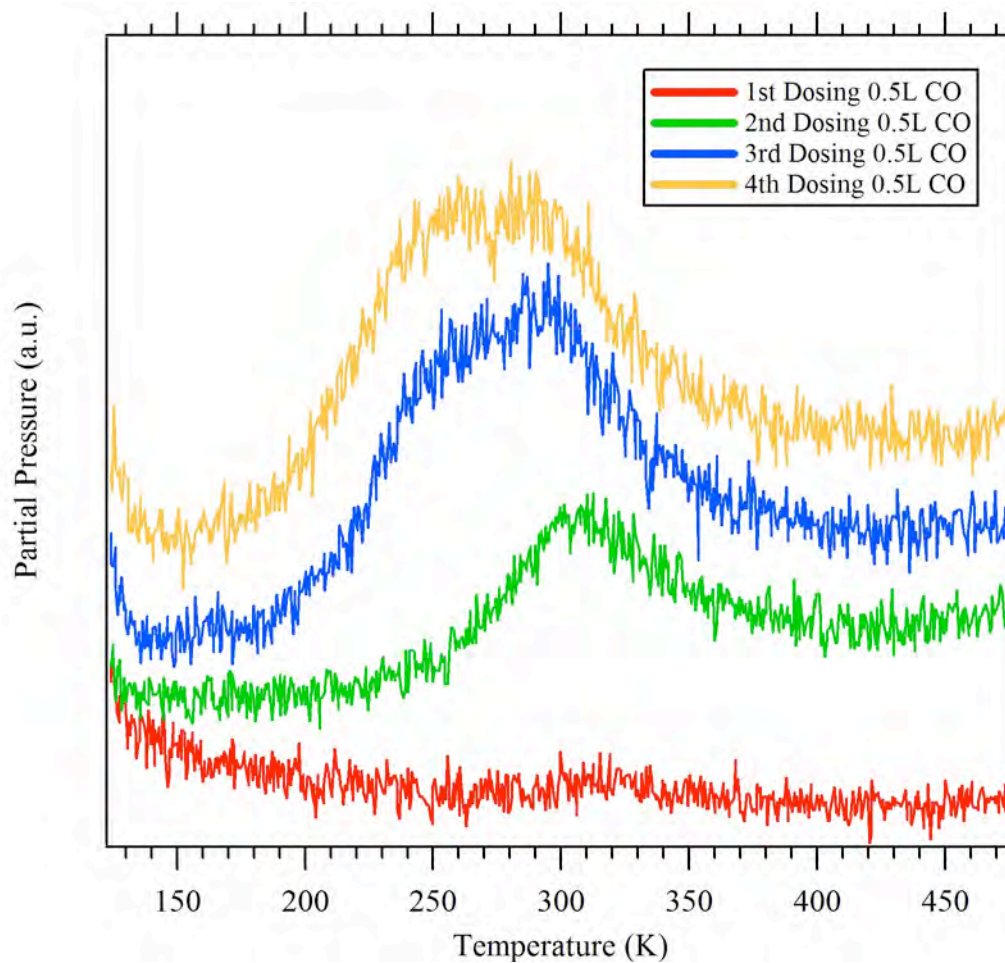


Figure 23: Partial pressure versus temperature curves of four consecutive dosing of 0.5L CO on Cr(110). All spectra were taken at a heating rate of 50°C/min and are offset for clarity.

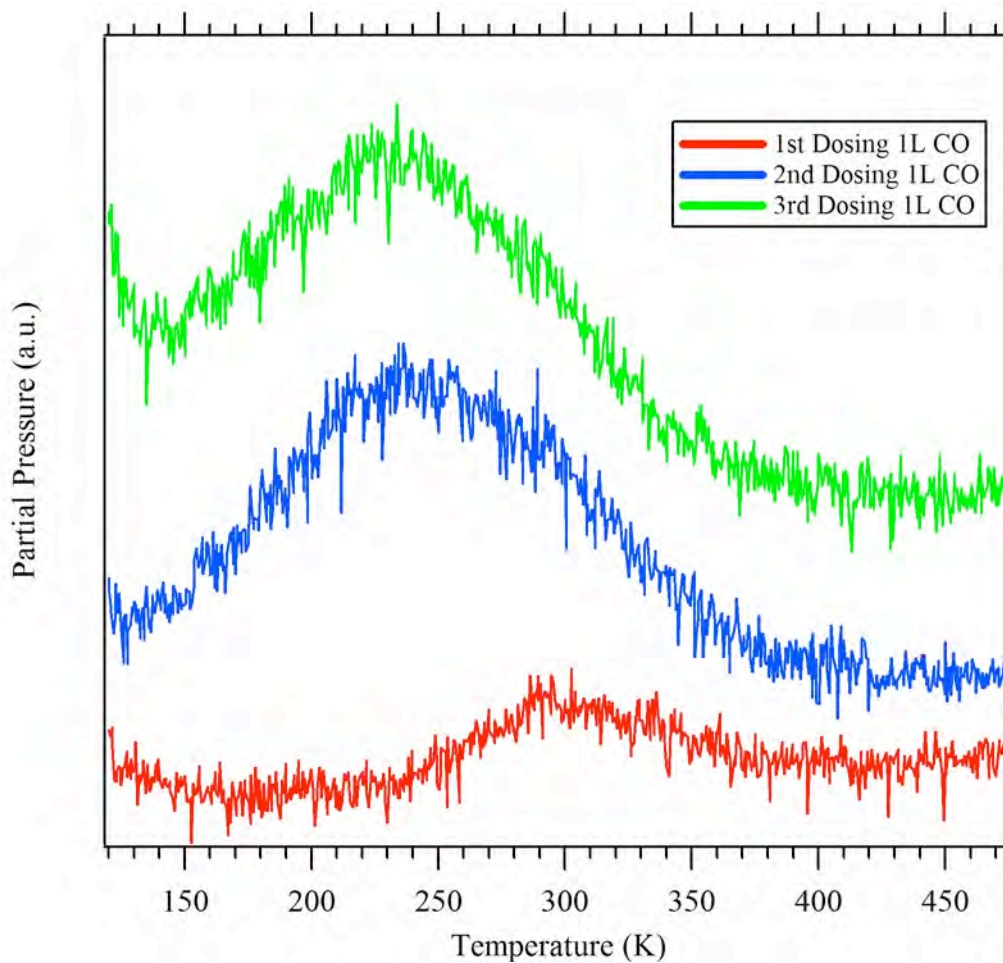


Figure 24: Partial pressure versus temperature curves of three consecutive dosing of 1L CO on Cr(110). All spectra were taken at a heating rate of 50°C/min and are offset for clarity.

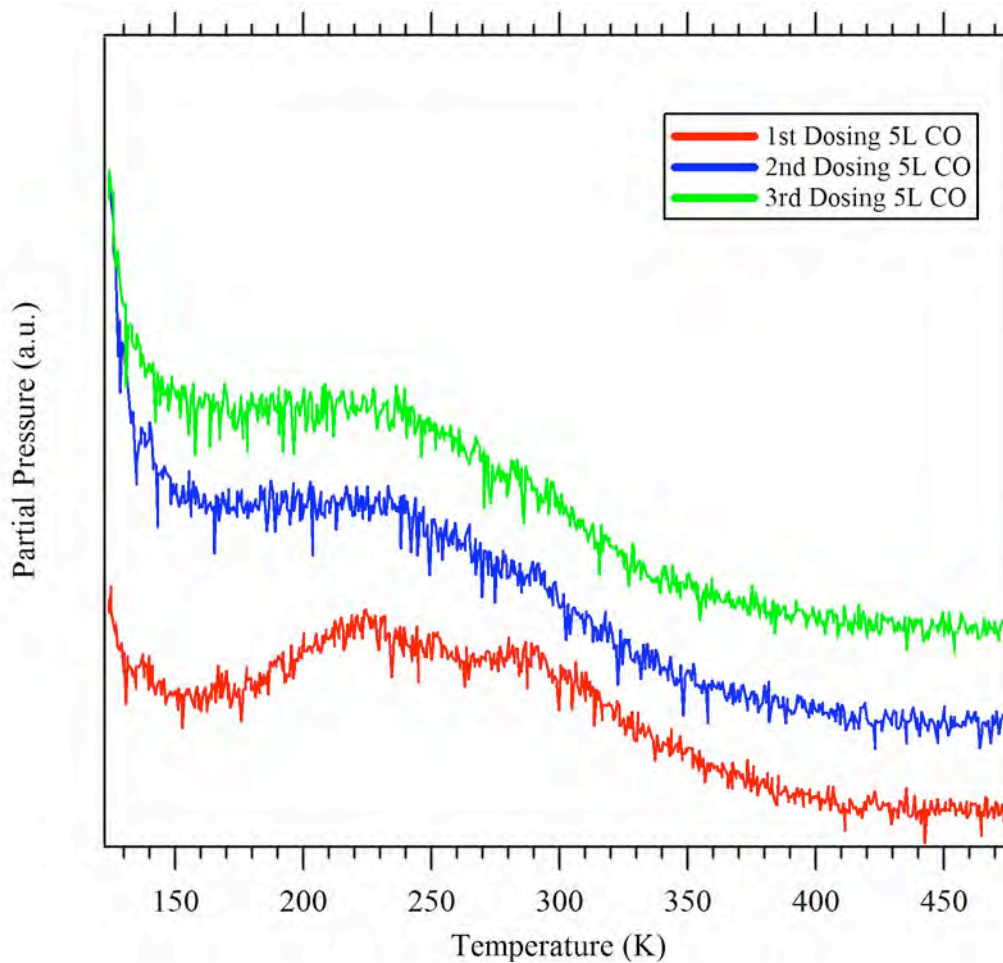


Figure 25: Partial Pressure vs. Temperature curves for three consecutive dosing of 5L CO on Cr(110). All spectra were taken at a heating rate of 50°C/min and are offset for clarity.

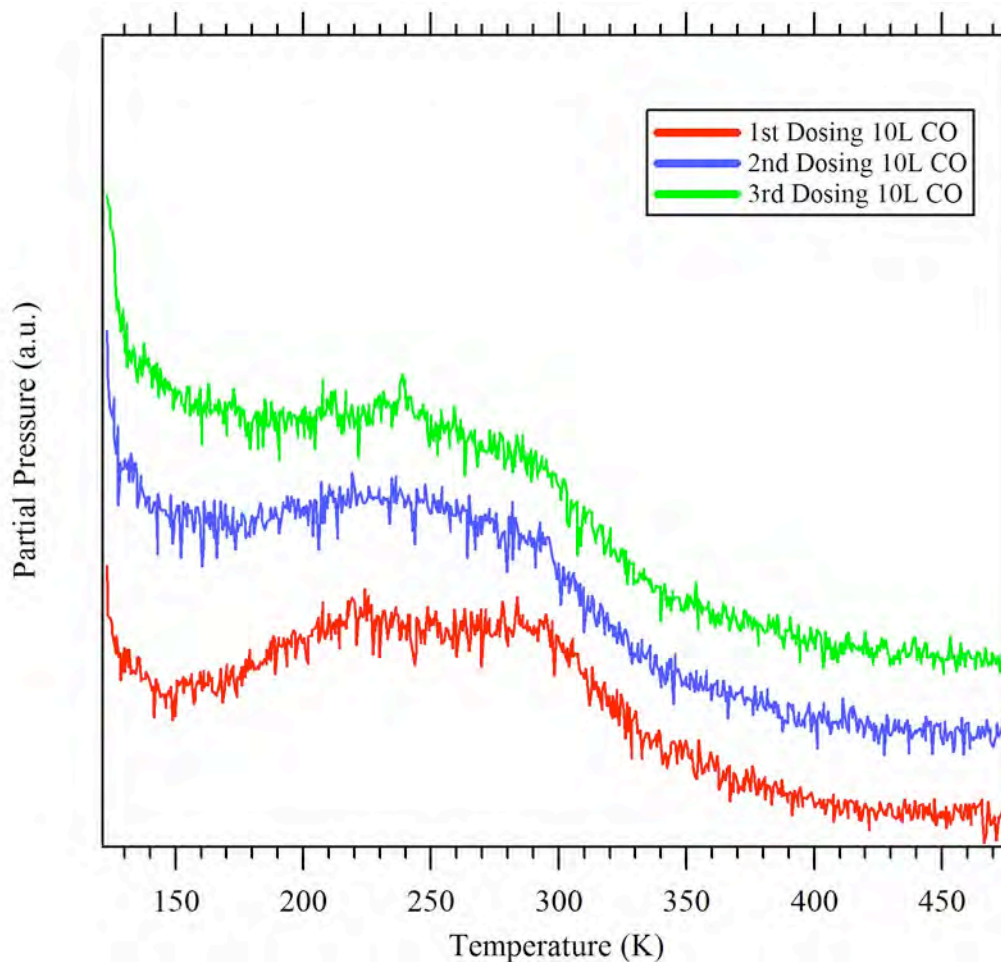


Figure 26: Partial pressure versus temperature curves for three consecutive dosing of 10L CO on Cr(110). All spectra were taken at a heating rate of 50°C/min and are offset for clarity.

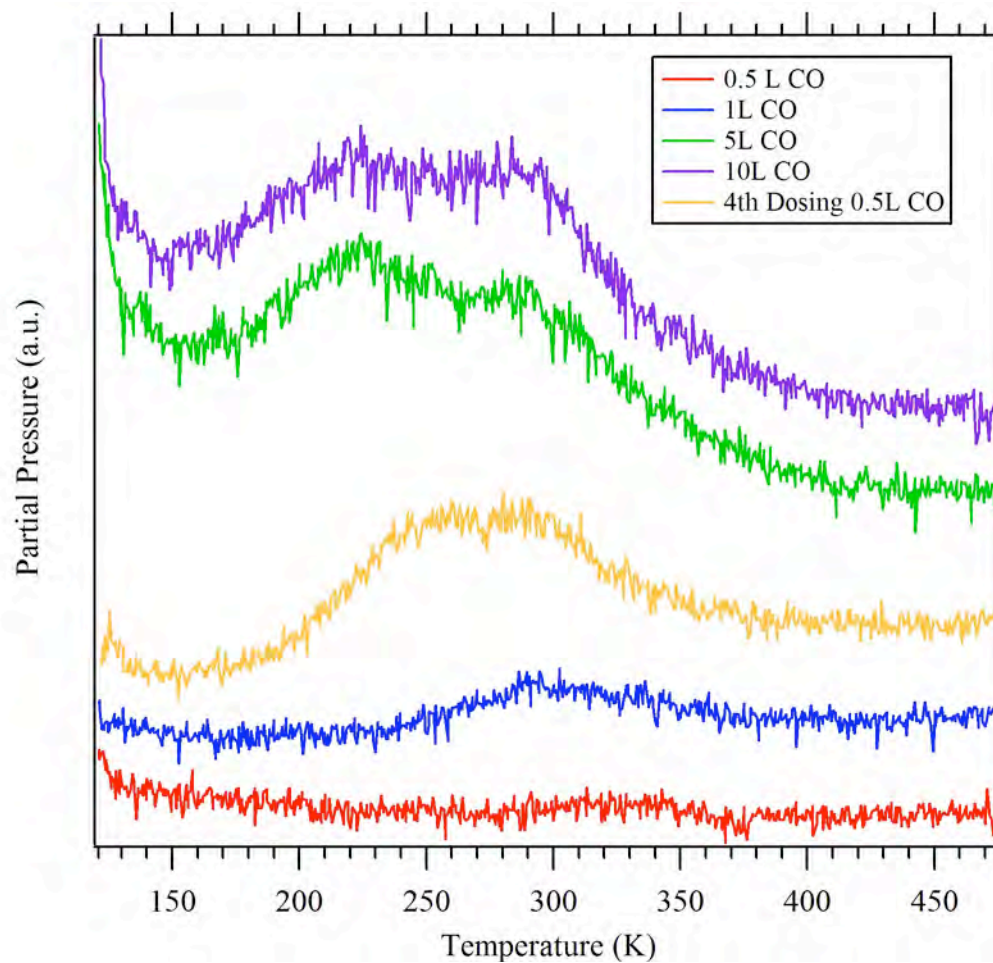


Figure 27: Partial pressure versus temperature curves of 5 different dosing of CO on Cr(110). All spectra were taken at a heating rate of 50°C/min and are offset for clarity.

C. CO-ADSORPTION OF CO WITH O₂

Measurements of the effect of co-adsorption of oxygen with CO on both the mixed Cr₂O₃(0001) and Cr(110) as well as clean Cr(110) were performed. For CO to adsorb onto the surface of Cr(110) it first needs to be cooled to at least 120 K. Oxygen was dosed at two different temperatures, 300 K and 120 K. In both cases O₂ was dosed before the CO was adsorbed. To see if oxygen affected the order structure of Cr(110) at 300 K, 1 L of O₂ was adsorbed onto the surface and LEED was performed, as seen in Figure 28. The quasi-hexagonal structure of Cr(110) is still observed, and weak spots not in registry with the Cr(110) spots are also observed. These extra spots are most likely from surface impurities of the nitrogen, which was discussed previously.

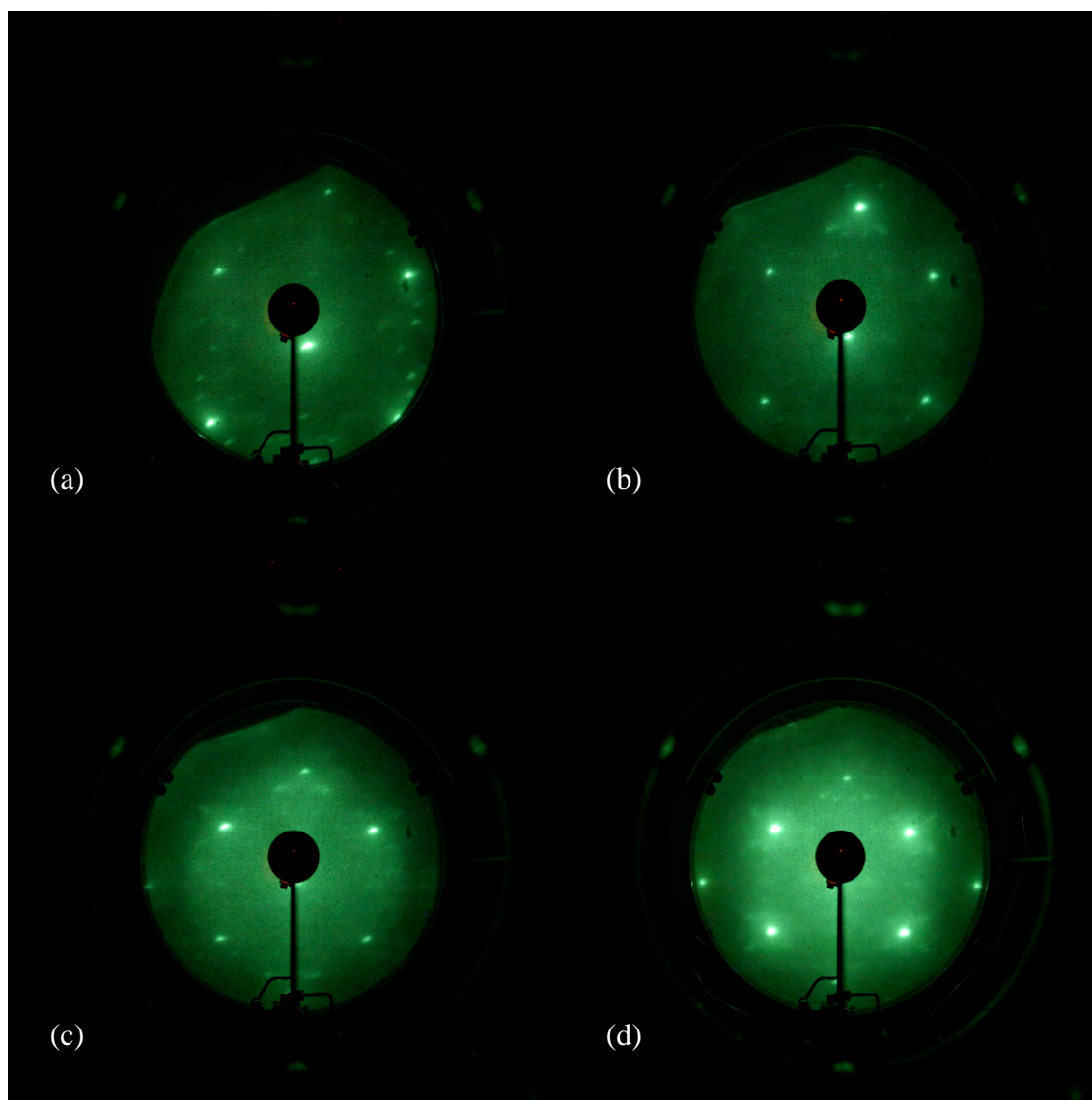


Figure 28: LEED patterns of Cr(110) with 1L of oxygen dosed at room temperature on the surface after twenty-two hot sputter/anneal cycles. Beam energies: a) 54.6 eV, b) 75.1 eV, c) 95.4 eV, d) 112.8 eV

Since oxygen is expected to dissociate on the Cr(110) surface, it is possible that molecular species such as CO₂, H₂O, or O₂ could desorb from the surface during the TPD measurements after co-adsorption of O₂ and CO. The co-adsorption TPD measurements were first performed on the mixed surface. The surface was first dosed with 1 L of O₂ at room temperature, the sample was cooled to 120 K, and the sample was then dosed with 1 L of CO. The TPD spectra of this sample for masses 12 (C), 15 (CH₃), 18 (H₂O), 28 (CO), 32 (O₂), and 44 (CO₂) are shown in Figure 29. The only mass with a significant peak is mass 28 (CO) at 220 K. A similar set of TPD spectra is observed for 1 L of O₂ dosed at 120 K followed by 1 L of CO dosed at 120 K, as shown in Figure 30. The primary difference between the two set of spectra is that the CO peak is shifted to 230 K for the oxygen dosed at 120 K. However, this is only a 10 K shift in the maximum of the desorption peak.

After six weeks of hot sputtering, the measurements were repeated on clean Cr(110). In Figure 31, 1 L of O₂ was dosed at room temperature and 1 L of CO was dosed at 120 K. As seen before, no other signal shows up other than mass 28 (CO) and the peak is located at 285 K. Two successive dosing sequences were completed after the first measurement without sputtering the surface of the sample in between. In Figure 32, both the second and third measurements show a smaller peak at 195 K and a very broad peak at 240 K.

In Figure 33, 1 L of O₂ along with 1 L of CO was co-adsorbed on the surface at 120 K. The peak is very broad and is centered at 260 K. This figure also shows no noticeable signal other than mass 28 (CO). Again, two more dosing sequences were completed without sputtering the sample in between trials in Figure 35. The second and

third measurements still show two peaks as in Figure 32 and are located at 195 K and 240 K.

A comparison of all co-adsorbed first trials of oxygen and CO along with a single measurement of 1L CO on Cr(110) is shown in Figure 35. With the addition of oxygen, the main peak shifts to lower temperatures as compared to CO adsorbed alone.

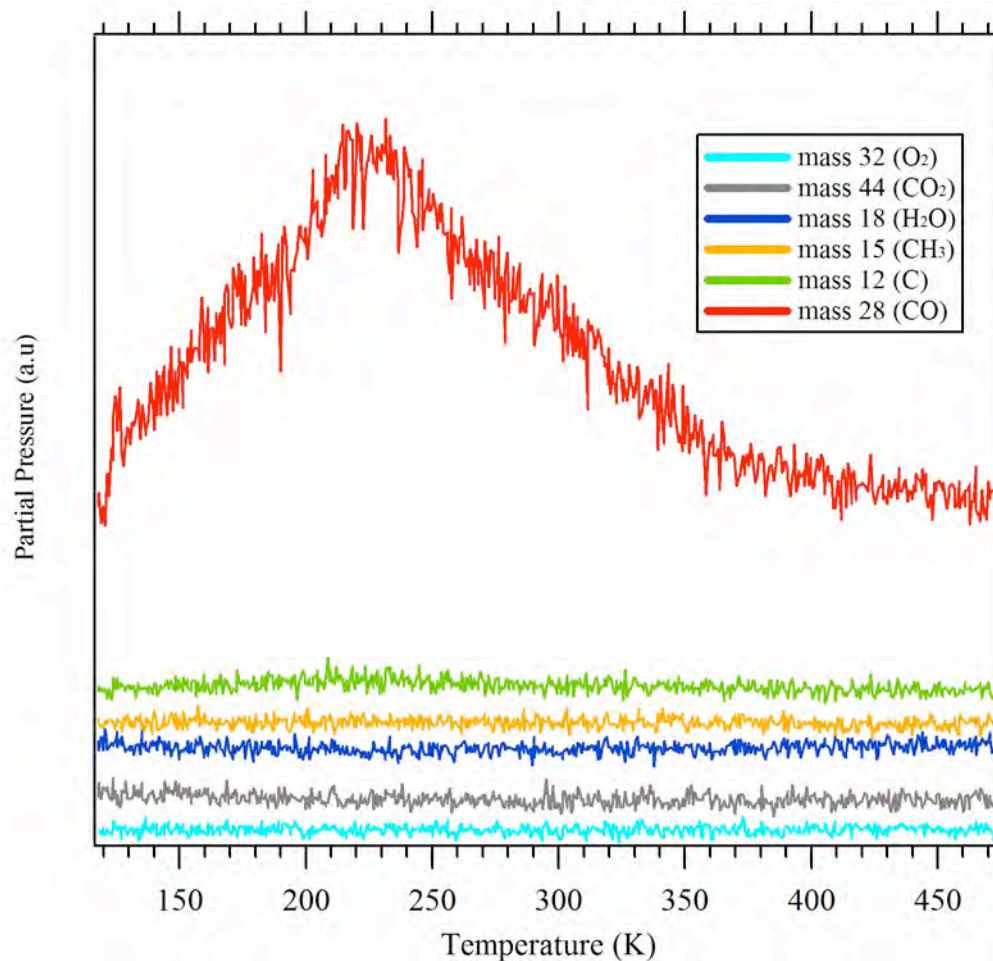


Figure 29: Partial pressure versus temperature curves of various masses for 1L O_2 dosed at room temperature and 1L CO dosed at 120K. Measurement was conducted on mixed $\text{Cr}_2\text{O}_3(0001)$ and $\text{Cr}(110)$. All spectra were taken at a heating rate of $50^\circ\text{C}/\text{min}$ and are offset for clarity.

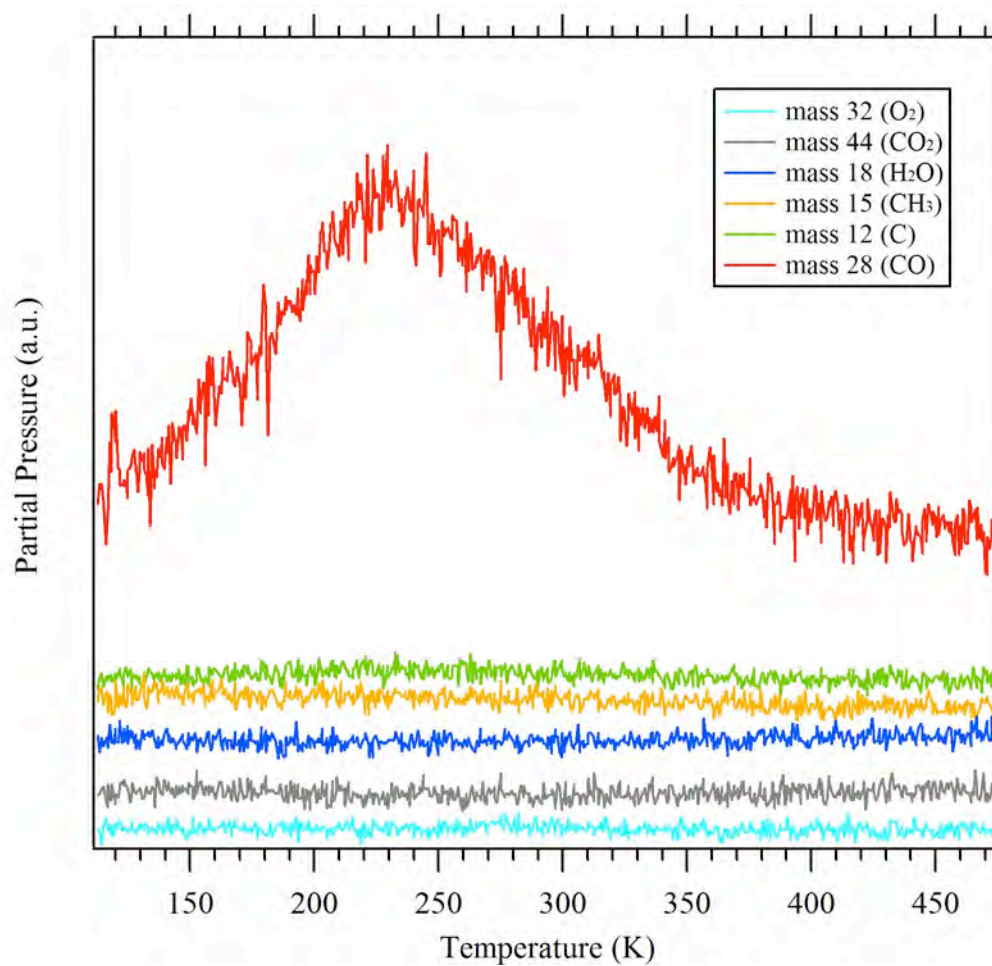


Figure 30: Partial pressure versus temperature curves for various masses of dosing 1L O_2 and 1L CO 120K. Measurement was conducted on mixed $\text{Cr}_2\text{O}_3(0001)$ and $\text{Cr}(110)$. All spectra were taken at a heating rate of $50^\circ\text{C}/\text{min}$ and are offset for clarity.

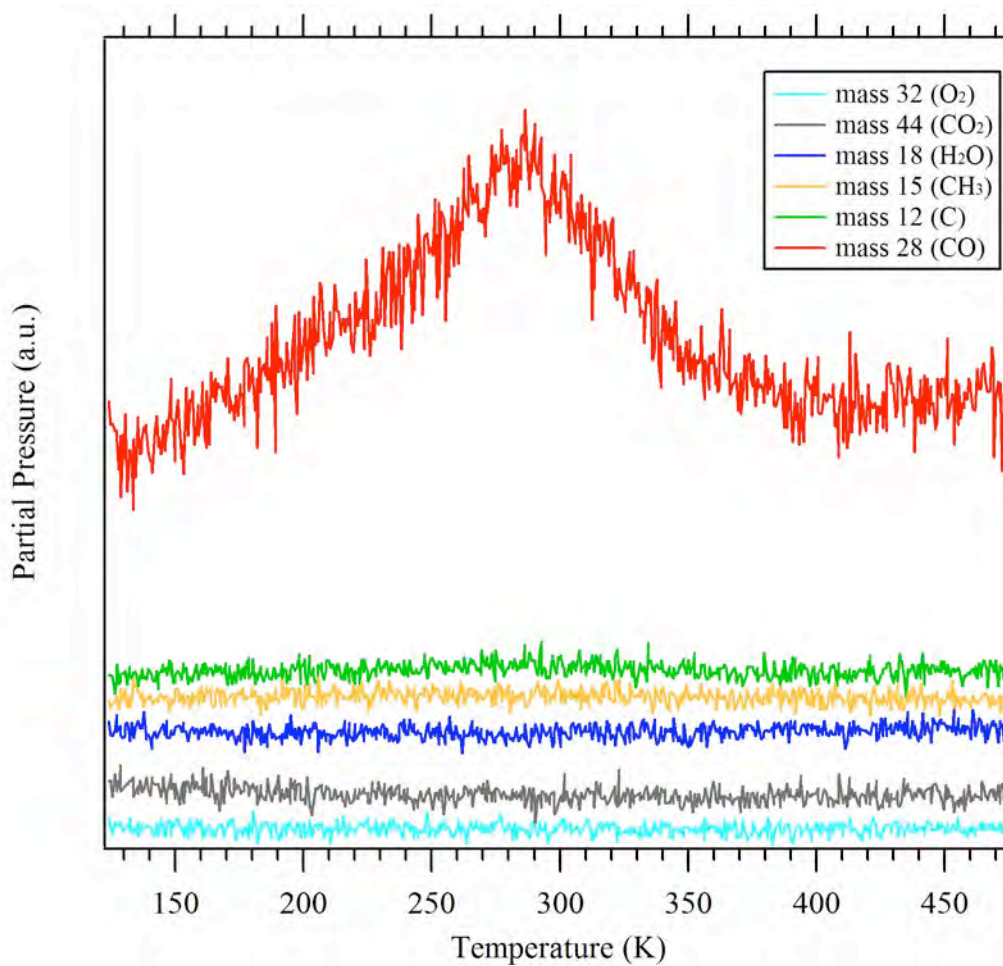


Figure 31: Partial pressure versus temperature curves of various masses for 1L O_2 dosed at room temperature and 1L CO dosed at 120K. Measurement was conducted on Cr(110). All spectra were taken at a heating rate of $50^\circ\text{C}/\text{min}$ and are offset for clarity.

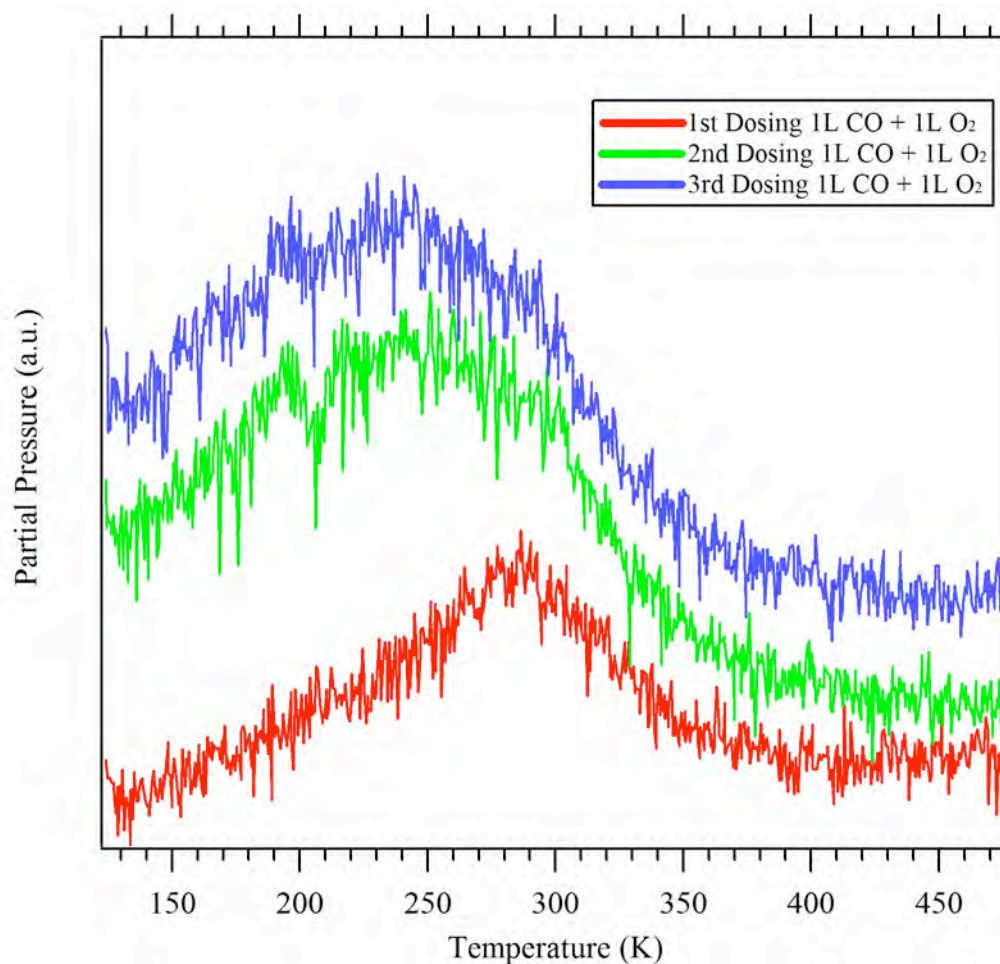


Figure 32: Partial pressure versus temperature curves of three consecutive dosing of 1L O₂ dosed at room temperature and 1L CO dosed at 120K. Measurements were conducted on Cr(110). All spectra were taken at a heating rate of 50°C/min and are offset for clarity.

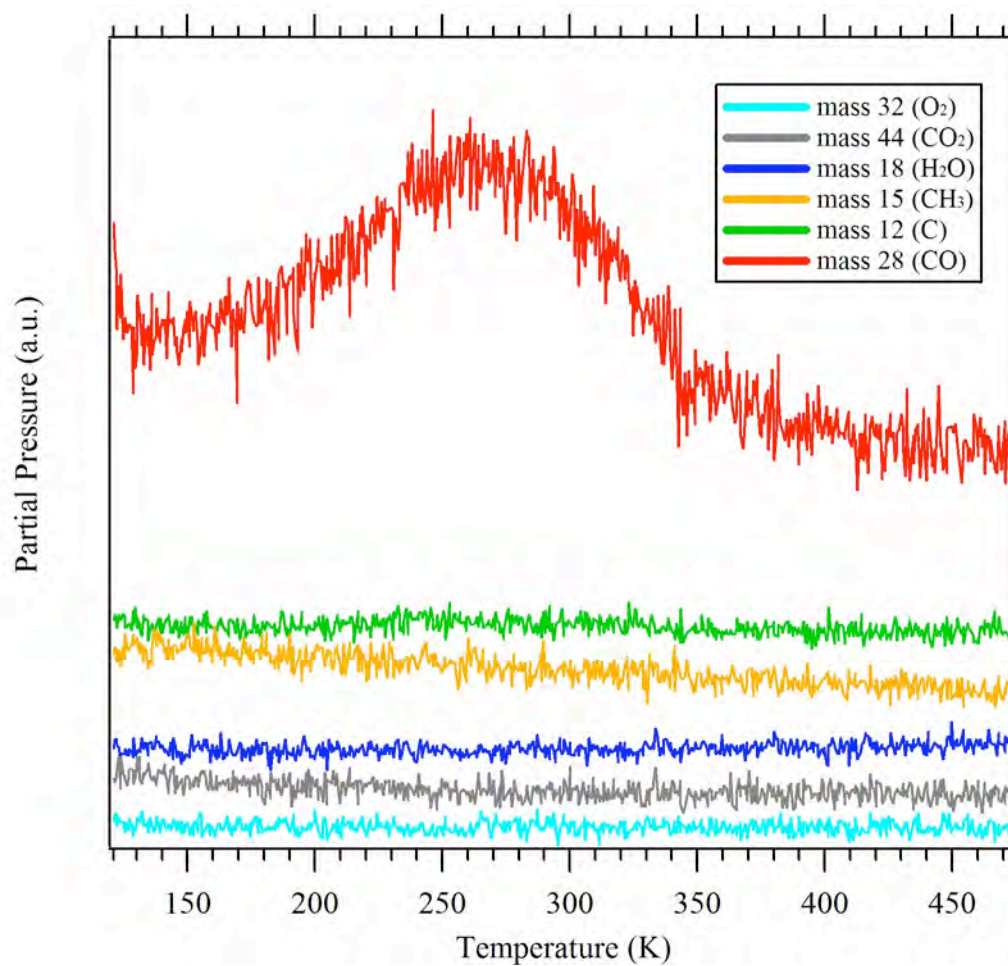


Figure 33: Partial pressure versus temperature curves of various masses for 1L O_2 and 1L CO dosed at 120K. Measurement was conducted on Cr(110). All spectra were taken at a heating rate of $50^\circ\text{C}/\text{min}$ and are offset for clarity.

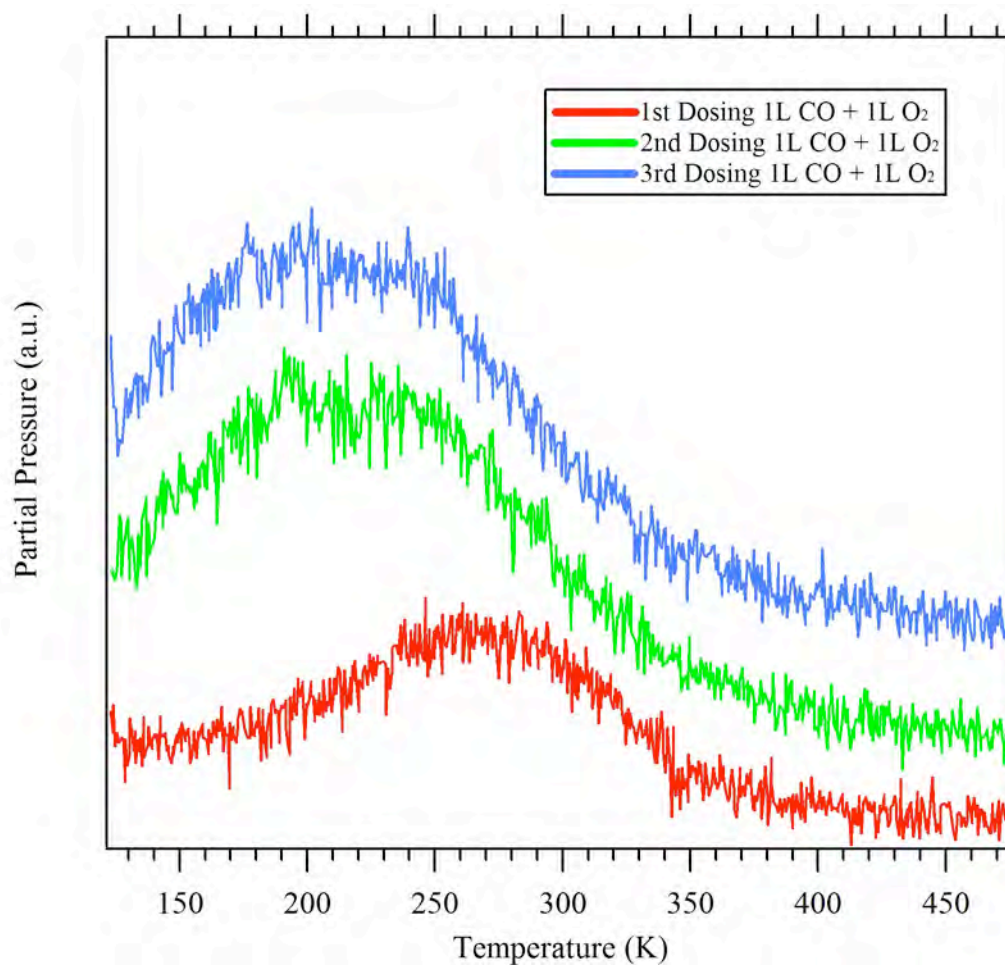


Figure 34: Partial pressure versus temperature curves of three consecutive dosing of 1L O₂ and 1L CO dosed at 120K. Measurements were conducted on Cr(110). All spectra were taken at a heating rate of 50°C/min and are offset for clarity.

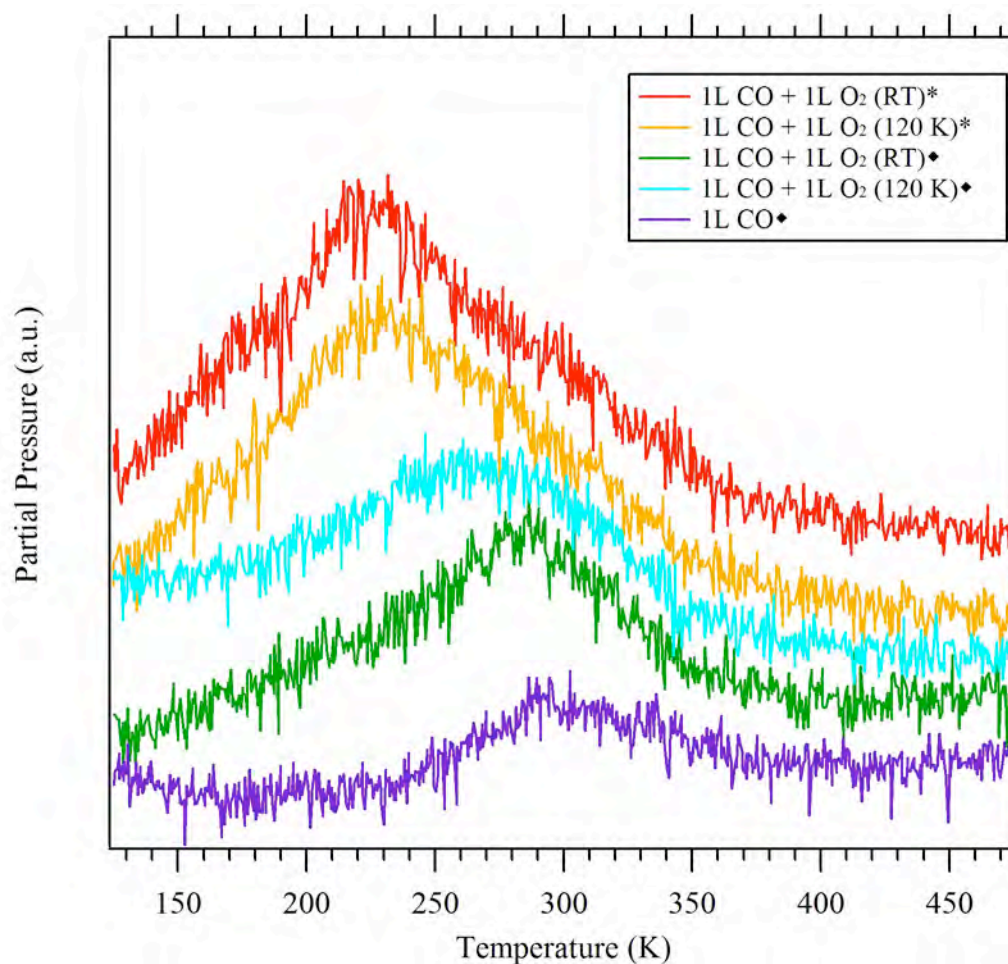


Figure 35: Partial pressure versus temperature curves of 1L CO on Cr(110) and various dosing of co-adsorbed oxygen and CO. All spectra were taken at a heating rate of 50°C/min and are offset for clarity.

*Mixed Cr₂O₃(0001) and Cr(110) surface

♦Clean Cr(110) surface

CHAPTER IV

DISCUSSION

The adsorption geometry and desorption pathway of CO on the Cr(110) surface is much different than for the Cr₂O₃(0001)/Cr(110) surface. The TPD spectra for a saturation coverage of CO on the oxide surface show a single well-defined peak at 175 K with a width of 20 °C for a heating rate of 50 °C/min. For the clean Cr(110) surface, adsorption of less than 0.5 L of CO results in almost no TPD signal, which indicates that the CO is reacting with the surface and dissociating instead of desorbing from the surface during the initial stages of adsorption. For doses greater than 0.5 L, multiple TPD peaks are observed, and the temperature range over which CO is observed to desorb is more than 200 °C. These results indicate that CO is only weakly chemisorbed on the Cr₂O₃(0001)/Cr(110) surface [16,17]. However, for the clean Cr(110) surface, the CO interaction is strong enough to cause the CO to dissociate and react with the surface for low coverages. The broad TPD peaks observed after the surface has reached a saturation of dissociated CO fragments, indicates that there are a broad range of binding sites and geometries for this surface.

A model for the adsorption geometry of CO on the Cr(110) surface is shown in Figure 1. Once the CO has dissociated on the Cr(110) surface, there are a large number of possible binding sites are available for the CO molecules to adsorb. This broadens the TPD peaks significantly since each adsorption site will have a different binding energy

associated with it. Previous EELS studies [2] have shown that CO chemisorbes on Cr(110) at 120 K as a molecule and dissociates during anneal. Because of this, a TPD spectrum for the adsorption of 0.5L of CO shows only a small desorption signal at 310 K. Up to a relative surface coverage of $\Theta < 0.25$, the CO molecules adsorb in a lying down configuration [2]. For larger coverages, CO adsorbs in both a lying down (α_1) and a standing up (α_2) geometry. When a larger amount of CO is dosed (1L), the molecules still begin to dissociate but enough “extra” CO is available to chemisorb and bind to the surface in one of the five different adsorption sites. The TPD signal shifts to a lower temperature of 290 K. Once the coverage is increased to more than 1.5L of CO, two broad peaks are seen in the TPD spectra. These two peaks come from both the CO species directly adsorbed onto the Cr metal (higher desorption temperature) and the CO molecules that are adsorbed on the dissociated carbon or oxygen on the surface (lower desorption temperature). EELS measurements have identified the dissociated species as clusters with varying configuration and are described as Cr_xO_y [2].

A sputter/anneal process was completed each day before any dosing was attempted to ensure that the surface of the Cr(110) crystal was clean. The first trial was always done on a clean sample. A sequential dosing was done for each coverage amount without sputter cleaning the sample between each trial. The TPD parameters for this thesis project never reached a high enough temperature for the dissociated C and O to leave the surface via recombination. Previous studies have shown that the recombination and desorption of CO occurs at 900 K [18], whereas in this work the maximum temperature that could be achieved for the TPD measurements was 700 K. Because of this some amount of dissociated CO remains on the surface after each TPD measurement.

For each subsequent dosing of CO, there is additional adsorption of CO onto the dissociated carbon and oxygen, resulting in an increase in the lower temperature desorption signal.

Oxygen was also co-adsorbed with CO at two different temperatures to see if the catalytically reactive surface of Cr(110) surface could produce the conversion of CO to CO₂. O₂ was first adsorbed at 300 K and CO at 120 K, after which TPD measurements were taken. The same procedure was repeated again but O₂ and CO were both adsorbed at 120 K. Both procedures produced similar TPD spectra. After reviewing the TPD spectra no signal for CO₂ was detected Figure 30 which indicates that the atomic oxygen has a higher affinity for forming Cr_xO_y species than for oxidizing the chemisorbed CO. When oxygen is dosed first, it dissociates onto the surface and blocks the binding sites available for the CO dissociation at low coverages. Therefore, most of the CO at the dose of 0.5 L dissociates for the oxygen predosed surface. This also results in a shift of the desorption signal to lower temperatures.

Another interesting consequence of oxygen predosing is that the TPD signal from the Cr₂O₃ regions of the mixed surface is gone. This indicates that oxygen co-adsorption on the Cr₂O₃(0001) surface blocks the adsorption of CO, which has also been measured previously [19].

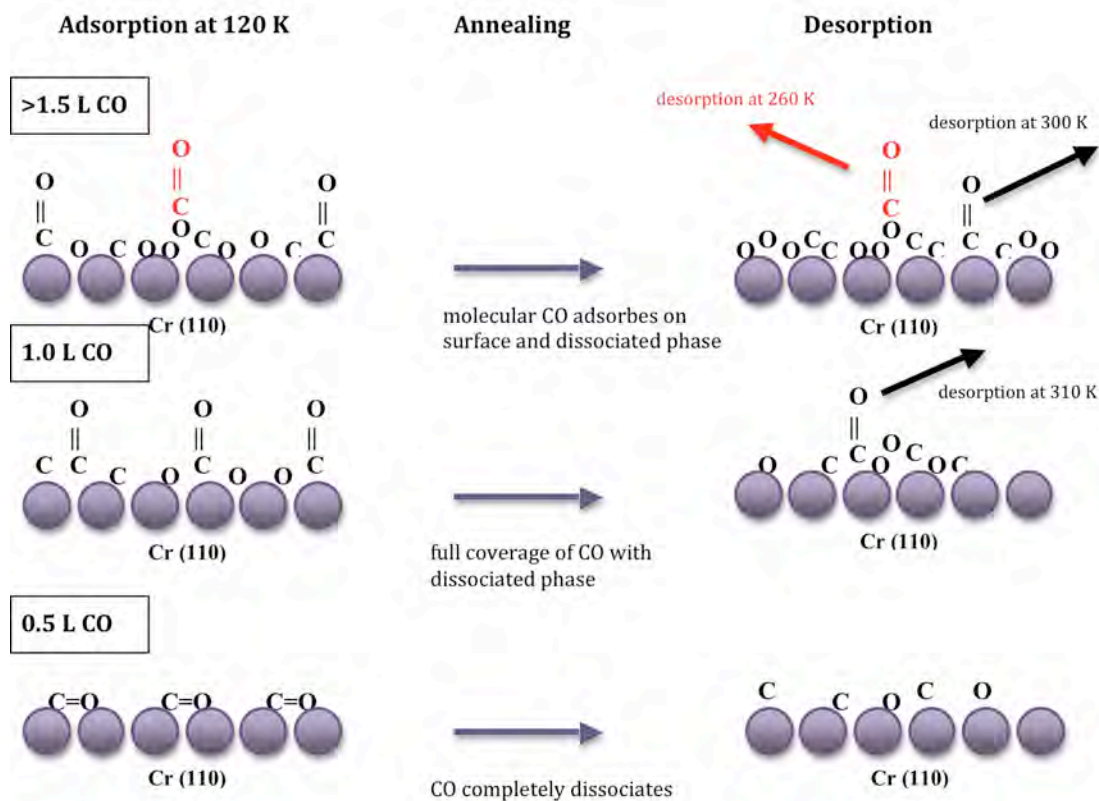


Figure 36: Diagram of the adsorption and dissociation for sequential dosing of 0.5 L CO on a Cr(110) surface.

CHAPTER V

CONCLUSIONS

The adsorption of CO on single-crystal metal surfaces has been extensively studied; however, only few measurements on the catalytic reactive Cr(110) surface have been published. This work concentrates on the temperature dependence of the adsorption and dissociation of CO on the Cr(110) surface and the influence of oxygen on the dissociation process. We have performed TPD and LEED studies of the adsorption of CO and CO co-adsorbed with oxygen on the Cr(110) surface. For low coverages CO dissociates on the Cr(110) surface. Once the CO has dissociated, there are a large number of possible binding sites are available for the CO molecules to adsorb. This broadens the TPD peaks significantly since each adsorption site will have a different binding energy associated with it. When a larger amount of CO is dosed (1L), the molecules still begin to dissociate but enough “extra” CO is available to chemisorb and bind to the surface in one of the five different adsorption sites. Once the coverage is increased to more than 1.5L of CO, two broad peaks are seen in the TPD spectra. These two peaks come from both the CO species directly adsorbed onto the Cr metal (higher desorption temperature) and the CO molecules that are adsorbed on the dissociated carbon or oxygen on the surface (lower desorption temperature).

Oxygen was also co-adsorbed with CO at two different temperatures to see if the catalytically reactive surface of Cr(110) surface could produce the conversion of CO to

CO₂. After reviewing the TPD spectra no signal for CO₂ was detected Figure 30 which indicates that the atomic oxygen has a higher affinity for forming Cr_xO_y species than for oxidizing the chemisorbed CO. It was also found that by predosing the surface with oxygen, the dissociation of CO in the initial stages of adsorption was suppressed.

REFERENCES

1. H.-J. Freund and M. Neumann, *Photoemission of Molecular Adsorbates*, Appl. Phys. A **47**, 3 (1988).
2. Neal D. Shinn and Theodore E. Madey, *CO Chemisorption on Cr(110): Evidence for a Precursor to Dissociation*, J. Chem. Phys. **83**, 11 (1985).
3. Neal D. Shinn, *Synchrotron photoemission study of CO chemisorption on Cr(110)*, The American Physical Society **38**, 17 (1988).
4. Neal D. Shinn and Theodore E. Madey, *Unusual C-O Bond Weakening on a Clean Metal Surface: CO on Cr(110)*, American Physical Society **53**, 26 (1984).
5. A.G. Baca, L.E. Klebanoff, M.A. Schulz, E. Paparazzo, and D.A. Shirley, *Dissociative Adsorption of CO and O₂ on Cr(100), Cr(110), and Cr(111) in the Temperature Range of 300-1175 K*, Surface Science **173**, 215 (1986).
6. S.P. Mehandru and Alfred B. Anderson, *Why CO Bonds Side-on at Low Coverage and Both Side-on and Upright at High Coverage on the Cr(110) Surface*, Surface Science **169**, L281 (1986).
7. M. Ohring, *Materials Science of Thin Films* (Academic Press, San Diego, CA, 2002).
8. G. Ertl, and J. Küppers, *Low Energy Electrons and Surface Chemistry* (VCH Verlagsgesellschaft mbH, D-6940 Weinheim, Federal Republic of Germany, 1985).
9. Electron: Mean Free Path, <http://www.philiphofmann.net/surflec/node11.html>
10. C. Kittel, *Introduction to Solid State Physics* (John Wiley & Sons, Inc., New York, 1996).
11. N. Ashcroft, and N. Mermin, *Solid State Physics* (W.B. Sanders Company, New York, 1976).
12. Quadrupole Mass Spectrometry, <http://www.files.chem.vt.edu/chem-ed/ms/quadrupo.html>

13. K. Kolasinski, *Surface Science: Foundations of Catalysis and Nano Science* (John Wilery & Sons, Ltd., West Sussex P019 1UD England, 2002).
14. N. Clark, M.S. Thesis, Texas State University-San Marcos, 2009.
15. M. Schmid, M. Pinczolits, W. Hebenstreit, and P. Varga, *The nitrogen-induced herringbone reconstruction of Cr(110)*, *Surface Science* **389**, L1140 (1997).
16. G. Arellano, M.S. Thesis, Texas State University-San Marcos, 2010.
17. U.A. Ditzinger, H. Neddermeyer, M. Neuber, and M. Neumann, *Adsorption and Reaction on Oxide Surfaces: CO and CO₂ on Cr₂O₃(111)*, *Ber. Bunsenges. Phys. Chem.* **96**, 15 (1992).
18. M.P. Engelhardt, T. Fuhrmann, G. Held, R. Denecke, and H.-P. Steinrück, *Adsorption of CO on ultrathin Cr layers on Ru(0001)*, *Surface Science* **512**, 107 (2002).
19. R. Denecke, B. Tränkenschuh, M.P. Engelhardt, and H.-P. Steinrück, *Adsorption kinetics of CO on Cr/Ru surfaces*, *Surface Science* **532-535**, 173 (2003).

VITA

Jennifer L. Walters was born December 15, 1980 to Glenda Kennedy in Houston, Texas. She has one younger brother James. Jennifer attended North Shore Senior High School where she graduated in 1999. While attending North Shore, she held leadership positions in FFA and Air Force JROTC.

After graduation Jennifer attended San Jacinto College in Houston. In the Spring of 2002 she transferred to Texas State University-San Marcos. While attending Texas State she worked full time for Fossil Inc. She also started undergraduate research for Dr. Carl Ventrice in Fall 2007. After balancing a full time work schedule and an academic schedule for 7 years she was able to graduate. She was awarded a Bachelor of Science in Physics in May 2008.

In Fall 2008 Jennifer began graduate school at Texas State University-San Marcos. She began graduate research in surface science and completed a study on the adsorption kinetics of carbon monoxide on Cr(110).

Permanent Address: 13418 Castilian Dr

Houston, TX 77015

This thesis was typed by Jennifer L. Walters.